The Future Is Fluid: Revolutionizing DOA Estimation With Sparse Fluid Antennas

He Xu, Tuo Wu, Ye Tian, *Senior Member, IEEE*, Ming Jin, *Senior Member, IEEE*, Wei Liu, *Senior Member, IEEE*, Qinghua Guo, *Senior Member, IEEE*, Maged Elkashlan, *Senior Member, IEEE*, Matthew C. Valenti, *Fellow, IEEE*, Chan-Byoung Chae, *Fellow, IEEE*, Kin-Fai Tong, *Fellow, IEEE*, and Kai-Kit Wong, *Fellow, IEEE*

***Abstract*—This paper investigates a design framework for sparse fluid antenna systems (FAS) enabling high-performance direction-of-arrival (DOA) estimation, particularly in challenging millimeter-wave (mmWave) environments. By ingeniously harnessing the mobility of fluid antenna (FA) elements, the proposed architectures achieve an extended range of spatial degrees of freedom (DoFs) compared to conventional fixed-position antenna (FPA) arrays. This innovation not only facilitates the seamless application of super-resolution DOA estimators but also enables robust DOA estimation, accurately localizing more sources than the number of physical antenna elements. We introduce two bespoke FA array structures and mobility strategies tailored to scenarios with aligned and misaligned received signals, respectively, demonstrating a hardware-driven approach to overcoming complexities typically addressed by intricate algorithms. A key contribution is a light-of-sight (LoS)-centric, closed-form DOA estimator, which first employs an eigenvalue-ratio test for precise LoS path number detection, followed by a polynomial root-finding procedure. This method distinctly showcases the unique advantages of FAS by simplifying the estimation process while enhancing accuracy. Numerical results compellingly verify that the proposed FA array designs and estimation techniques yield an extended DoFs range, deliver superior DOA accuracy, and maintain robustness across diverse signal conditions.**

***Index Terms*—Sparse fluid antennas (FA) array, direction-of-arrival (DOA) estimation, aligned received signals, misaligned received signals, polynomial root finding.**

Received 3 July 2025; revised 15 November 2025; accepted 26 January 2026. Date of current version 10 February 2026. This work was supported in part by Zhejiang Provincial Natural Science Foundation of China under Grant LQN26F010011, in part by the Natural Science Foundation of China under Grant 62571286, in part by the Natural Science Foundation of Ningbo Municipality under Grant 2024J232, and in part by The Hong Kong Polytechnic University Start-Up Fund under Project P0053642. The work of Tuo Wu was supported by Hong Kong Research Grants Council under the Area of Excellence Scheme under Grant AoE/E-101/23-N. The work of Kin-Fai Tong was supported by The Hong Kong Metropolitan University, Staff Research Startup Fund, under Grant FRSF/2024/03. The work of Kai-Kit Wong was supported by the Engineering and Physical Sciences Research Council (EPSRC) under Grant EP/W026813/1. The associate editor coordinating the review of this article and approving it for publication was M. Mezzavilla. *(Corresponding authors: Tuo Wu; Kai-Kit Wong.)*

He Xu is with the School of Cyber Science and Engineering, Ningbo University of Technology, Ningbo 315211, China (e-mail: xuhebest@sina.com).

Tuo Wu is with the State Key Laboratory of Terahertz and Millimeter Waves, City University of Hong Kong, Hong Kong, China (e-mail: tuowu2@cityu.edu.hk).

Ye Tian and Ming Jin are with the Faculty of Electrical Engineering and Computer Science, Ningbo University, Ningbo 315211, China (e-mail: tianye1@nbu.edu.cn; jinming@nbu.edu.cn).

Wei Liu is with the Department of Electrical and Electronic Engineering, The Hong Kong Polytechnic University, Hong Kong (e-mail: wei2.liu@polyu.edu.hk).

Qinghua Guo is with the School of Engineering, University of Wollongong, Wollongong, NSW 2522, Australia (e-mail: qguo@uow.edu.au).

Maged Elkashlan is with the School of Electronic Engineering and Computer Science, Queen Mary University of London, E1 4NS London, U.K. (e-mail: maged.elkashlan@qmul.ac.uk).

Matthew C. Valenti is with the Lane Department of Computer Science and Electrical Engineering, West Virginia University, Morgantown, WV 26506 USA (e-mail: valenti@ieee.org).

Chan-Byoung Chae is with the School of Integrated Technology, Yonsei University, Seoul 03722, South Korea (e-mail: cbchae@yonsei.ac.kr).

Kin-Fai Tong is with the School of Science and Technology, The Hong Kong Metropolitan University, Hong Kong, SAR, China (e-mail: ktong@hkmu.edu.hk).

Kai-Kit Wong is with the Department of Electronic and Electrical Engineering, University College London, WC1E 6BT London, U.K., and also with the Yonsei Frontier Laboratory, Yonsei University, Seoul 03722, South Korea (e-mail: kai-kit.wong@ucl.ac.uk).

Digital Object Identifier 10.1109/TWC.2026.3660268

I. Introduction

THE sixth generation (6G) wireless communication systems are anticipated to meet unprecedented requirements for high data rates, ultra-low latency, and spectral efficiency to support emerging applications such as immersive extended reality, holographic communications, and autonomous systems [1]. Conventional multiple-input multiple-output (MIMO) architectures, despite their proven effectiveness in current networks, exhibit inherent limitations in scalability and adaptability for 6G scenarios. Fluid antenna systems (FAS) have recently emerged as a paradigm-shifting technology that addresses these fundamental limitations through physically reconfigurable antenna structures [2], [3], [4]. By enabling dynamic port selection and position optimization within a constrained physical space, FAS fundamentally decouples the radiation characteristics from fixed hardware constraints, thereby facilitating adaptive spatial multiplexing and diversity exploitation [5]. This architectural innovation enables FAS to achieve enhanced degrees of freedom, improved interference management, and superior channel utilization across diverse propagation environments. Recent investigations have demonstrated FAS's potential advantages in various aspects of wireless communications, including capacity enhancement, reliability improvement, and resource utilization optimization [6], [7], [8], [9], [10], [11], [12], [13], [14], [15].

The concept of the fluid antenna (FA), sometimes referred to as a movable antenna (MA) [5], centers on the ability to dynamically reconfigure the position or activation of

antenna elements to optimize communication performance. While some early prototypes explored fluidic implementations using conductive liquids within precision-controlled structures [2], the broader FA framework encompasses a variety of technologies—including electronically switchable arrays, reconfigurable metasurfaces [16], and spatially distributed antenna pixels [17]—that achieve the same functional flexibility without any physical movement. This reconfigurability marks a key distinction from conventional fixed-position antenna (FPA) arrays, where element locations are permanently static. **By enabling dynamic control over which spatial points act as radiating elements, FA systems effectively expand the spatial degrees of freedom (DoFs), creating a virtual aperture that surpasses the physical limitations of traditional antenna arrays** [12]. This spatial DoFs expansion directly translates to enhanced communication performance metrics, including improved channel capacity, increased signal-to-noise ratio, and more effective interference mitigation [9]. While conceptually comparable to sparse antenna array implementations [18], [19], [20], [21], FAS offer a critical operational advantage: they adaptively reconfigure spatial distributions in response to dynamic channel conditions, whereas sparse FPA arrays rely exclusively on predetermined element spacings that remain fixed throughout operation. This dynamic adaptability enables FA-based systems to achieve superior channel utilization efficiency without the mutual coupling limitations that typically constrain closely-spaced antenna elements, thereby presenting significant performance advantages across diverse wireless communication applications [22], [23], [24], [25], [26], [27], [28], [29], [30].

Beyond general communication enhancements, the expanded spatial DoFs and virtual aperture extension afforded by FAS present particularly compelling advantages for direction-of-arrival (DOA) estimation. DOA estimation is a foundational task in array signal processing, supporting critical functions such as target localization in radar and sonar detection systems, channel estimation, and downlink precoding in wireless communication systems [31], [32], [33]. Conventional DOA estimation techniques predominantly rely on FPAs. While numerous DOA estimation methods have been developed for FPA arrays, including linear prediction-based methods [34], [35], subspace-based methods [36], [37], sparse signal reconstruction-based methods [38], [39], deep learning-based methods [40], [41], and statistical inference-based methods [42], [43], these approaches are inherently constrained by the fixed spatial DoFs and limited flexibility of FPAs. These limitations often restrict their ability to achieve high-resolution DOA estimation, especially in complex scenarios with multiple closely spaced sources or underdetermined conditions.

In stark contrast, FAS, by strategically controlling element positions, can achieve substantially larger virtual apertures than physically possible with equivalent-sized FPA arrays, directly improving angular resolution capabilities and **achieving super-resolution**. Moreover, this controllable expansion of spatial diversity **enables stable operation in underdetermined DOA estimation scenarios**, allowing the accurate localization of more signal sources than the number of physical antenna elements–a capability traditionally unattainable with conventional arrays of comparable physical dimensions. This ability to **achieve high-performance DOA estimation through innovative hardware design, which would otherwise necessitate algorithms of high computational complexity**, distinctly **reflects the unique characteristics and advantages of FAS**. Additionally, the flexible element spacing possible with FAS can be optimized to minimize mutual coupling effects that typically degrade estimation accuracy in densely packed arrays, while simultaneously maintaining the extended aperture necessary for high-resolution parameter estimation. These inherent advantages position FA-based DOA estimation as a promising solution to overcome fundamental limitations in conventional array processing techniques and unlock new potentials for high-performance spatial signal processing.

However, realizing the full potential of FAS for DOA estimation is not without its hurdles. The practical implementation of FA-based DOA estimation must contend with several intrinsic challenges. Firstly, the very mobility that grants FAs their advantage is often constrained by physical limitations on the number of movements possible within the typically short observation times required for DOA estimation, where the direction information is assumed to be quasi-static [32], [44], [45], [46]. Secondly, translating these limited movements into a substantial and, crucially, consecutive expansion of spatial DoFs, essential for many super-resolution algorithms, demands meticulous design of both the FA array geometry and its mobility strategy. Thirdly, particularly in mmWave bands targeted for future wireless systems, the presence of non-line-of-sight (NLoS) propagation paths can introduce significant multipath interference, complicating the accurate extraction of LoS signal parameters. Fourthly, the dynamic nature of the FA array necessitates robust and computationally efficient DOA estimation algorithms capable of processing the potentially time-varying array manifold. Finally, while FAS offer the potential to mitigate mutual coupling through element spacing, this remains a design consideration to ensure the integrity of the received signals across different antenna positions.

The aforementioned challenges are further compounded in scenarios involving misaligned received signals. To clarify this distinction, we formally define *aligned received signals* as scenarios where the signals received at different FA positions are phase and time synchronized after each movement, as if they were received simultaneously by a larger, virtual array. This alignment enables direct combination of received samples from different positions to form a coherent virtual array with extended spatial response. Conversely, *misaligned received signals* refer to scenarios where such phase and time synchronization cannot be maintained across FA movements, preventing direct signal combination due to independent signal variations at each position.

While pilot-based communication systems may employ mechanisms to ensure signal alignment at the receiver after each FA movement, such alignment cannot be guaranteed in many critical DOA application contexts, including radar, sonar detection, or opportunistic signal-based collaborative positioning. In these non-cooperative or passive sensing scenarios, the signals received after successive FA movements are inherently

misaligned due to the unknown and independent nature of the signal sources. This fundamental misalignment can severely degrade, or even nullify, the benefits accrued from spatial DoFs expansion if not appropriately addressed, rendering accurate DOA parameter estimation significantly more complex and demanding more sophisticated array designs and signal processing techniques.

To address these multifaceted challenges, this paper introduces novel FA array structures and corresponding mobility mechanisms designed for DOA estimation under both aligned and misaligned received signal conditions. Complementing these hardware-centric innovations, we propose a low-complexity polynomial root-finding algorithm for robust DOA estimation, further enhanced by an effective method for detecting the number of line-of-sight (LoS) paths. Our simulation results demonstrate that these integrated solutions yield a significantly expanded range of consecutive spatial DoFs, thereby enabling high-performance underdetermined DOA estimation with notable improvements in accuracy. The primary contributions of this work are detailed as follows:

- ***Optimized Sparse Array for Aligned Signals:*** Taking the scenario of aligned received signals and the limited number of movements into consideration, a sparse FA array structure consisting of two subarrays with large element spacing is first designed, and further optimized by applying different step size to the two subarrays, a significantly increased consecutive spatial DoFs is achieved, which efficiently avoids the negative effects of array mutual coupling and allows most existing super-resolution estimators to be applied directly, finally facilitating the achievement of high-performance underdetermined DOA estimation.
- ***Generalized Hybrid Array for Misaligned Signals:*** A generalized FA array composed of an FPA array and an FA array with large element spacing is designed for misaligned received signals. It is demonstrated that by introducing a suitable PFA array, the array output data can be aligned in the second-order statistical domain and still provide increased consecutive spatial DoFs. Meanwhile, this design is also applicable to scenarios with aligned received signals, offering higher universal applicability.
- ***LoS-Centric Closed-Form DOA Estimator:*** Considering the propagation characteristic of mm-wave signals, we couple the impact of NLoS signals into the interference-plus-noise term, and then propose an approach for estimating the number of LoS paths/targets based on eigenvalue detection. Finally, a closed-form solution for DOA estimation is achieved by applying the polynomial root finding algorithm. Compared to the DOA estimation schemes that detect all paths, our scheme can provide significantly improved estimation accuracy and robustness.
- ***Comprehensive Performance Analysis and Validation:*** The performance in terms of estimation accuracy, computational complexity, capacity for underdetermined DOA estimation and the appropriate Cramér-Rao Bound (CRB) for the considered scenarios are analyzed/provided. Extensive simulations under various FA array configurations are performed, which not only validate the effectiveness and superiority of the proposed solutions, but also facilitate their practical engineering implementation.

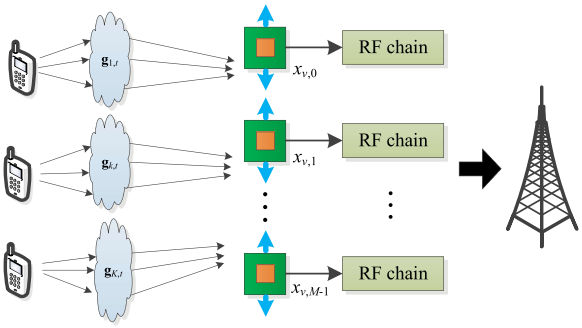

Fig. 1. Illustration of FA array enabled DOA estimation system.

This paper is organized as follows. In Section II, the mm-wave signal model for FA array enabled DOA estimation is introduced, where both aligned and misaligned received signals are considered. In Section III, two sparse FA array structures and their corresponding mobility mechanisms are designed and analyzed. In Section IV, we first introduce the LoS number detection based DOA estimation algorithms in detail, and then analyze their corresponding performance. Simulation results and main observations are provided in Section V, and conclusions are drawn in Section VI.

Notations: Bold symbols in small letter and capital letter represent vectors and matrices, respectively. a and $\mathcal{L}$ represent a scaler and a set, respectively. The superscripts $(\cdot)^T$, $(\cdot)^H$ and $(\cdot)^*$ stand for the transpose, conjugate transpose and conjugate, respectively. $\mathbb{E}\{\cdot\}$ denotes the statistical expectation operation, $\mathrm{diag}\,(\cdot)$ and $\mathrm{blkdiag}\,(\cdot)$ are the diagonalization and block diagonalization operations, respectively. $\mathrm{vec}(\cdot)$ represents the vectorization operator, which converts a matrix into a vector by stacking all of its columns on top of each other. $\otimes$ denotes the Kronecker product, and $\mathrm{spec}(\cdot)$ the eigenvalues of a matrix. $\mathrm{Peak}(\cdot)$ returns the index corresponding to the first peak in the bracket. $\mathbf{J}_M$ denotes an $M \times M$ exchange matrix, and $\mathbf{I}_M$ an $M \times M$ identity matrix. For two sets $\mathcal{L}$ and $\mathcal{C}$, $\mathcal{L} \cup \mathcal{C}$ denote their union, and finally, $\mathcal{CN}(\mathbf{0}, \sigma_n^2 \mathbf{I}_M)$ indicates a complex Gaussian distribution with zero mean and variance σ_n^2.

II. Signal Model

Consider a mmWave narrowband system equipped with an M-element linear FA array,[1] as illustrated in Fig. 1. The system simultaneously receives signals from K single-antenna signal sources (referred to as targets throughout this paper), which can represent transmitting users in communication systems, radar targets, or any radiating objects whose DOAs are to be estimated. Let $x_{v,m}$ denote the position of the m-th FA element after the v-th displacement, where $m \in \{0, \ldots, M-1\}$ and $v \in \{0, \ldots, G\}$.

At mmWave frequencies, the propagation channel is characterized by its DoA and complex gain [47], [48], [49]. Measurement studies have confirmed that angular parameters remain relatively stable, while small-scale fading coefficients change more rapidly [50], [51], [52]. Throughout the G

[1]The term FA array hereafter denotes any array that contains movable radiating elements. When the received signals are misaligned, a subset of fixed-position antennas (FPAs) can be included to form the required consecutive spatial DoFs; see Section III for details.

consecutive movements, we therefore treat the path gains as quasi-static and neglect FA positioning errors, which typically remain below one-hundredth of the wavelength [53]. Under these assumptions, the channel from the k-th signal source observed at the t-th snapshot after the v-th displacement can be expressed as

$$\mathbf{h}_{k,v,t} = \sum_{l=1}^{L} g_{k,l,t}\mathbf{a}_v\left(\theta_{k,l}\right), k \in [1,K], v \in [0,G], \quad (1)$$

where $g_{k,1,t}$ and $g_{k,l,t}$ ($l \neq 1$) denote the complex Gaussian channel gains for the LoS and NLoS paths of the k-th target at the t-th snapshot, respectively. Here, L represents the maximum number of paths considered for any target (or a common modeling parameter for the number of paths per target), and $\mathbf{a}\left(\theta_{k,l}\right)$ is the array manifold vector corresponding to the DOA $\theta_{k,l}$ of the l-th path of the k-th target, which can be expressed as

$$\mathbf{a}_v\left(\theta_{k,l}\right) = \left[e^{-jx_{v,0}\varpi_{k,l}}, \ldots, e^{-jx_{v,M-1}\varpi_{k,l}}\right]^T, \quad (2)$$

where $\varpi_{k,l} = 2\pi \sin\theta_{k,l}/\lambda$, and λ is the carrier wavelength.

To facilitate subsequent analysis and system modeling, the uplink channel $\mathbf{h}_{k,v,t}$ can be expressed in a compact matrix-vector form as

$$\mathbf{h}_{k,v,t} = \mathbf{A}_{k,v}\mathbf{g}_{k,t}, \quad (3)$$

where

$$\mathbf{A}_{k,v} = \left[\mathbf{a}_v\left(\theta_{k,1}\right), \ldots, \mathbf{a}_v\left(\theta_{k,L}\right)\right], \quad (4)$$

$$\mathbf{g}_{k,t} = \left[g_{k,1,t}, \ldots, g_{k,L,t}\right]^T. \quad (5)$$

Let $s_{k,v,t}$ denote the signal transmitted by the k-th target ($k \in [1,K]$) after the v-th movement at the t-th snapshot. We assume these signals are of equal power and are uncorrelated with each other. Under these assumptions, the received signal vector at the FA array, denoted by $\mathbf{y}_{v,t}$, can be expressed as

$$\begin{aligned}\mathbf{y}_{v,t} &= \left[\mathbf{h}_{1,v,t}, \ldots, \mathbf{h}_{K,v,t}\right]\mathbf{s}_{v,t} + \mathbf{n}_{v,t} \\ &= \left[\mathbf{A}_{1,v}, \ldots, \mathbf{A}_{K,v}\right]\mathbf{G}\mathbf{s}_{v,t} + \mathbf{n}_{v,t} \\ &= \left[\mathbf{A}_{1,v}, \ldots, \mathbf{A}_{K,v}\right]\bar{\mathbf{s}}_{v,t} + \mathbf{n}_{v,t} = \mathbf{A}_v\bar{\mathbf{s}}_{v,t} + \mathbf{n}_{v,t}, \end{aligned} \quad (6)$$

where $\bar{\mathbf{s}}_{v,t} = \mathbf{G}\mathbf{s}_{v,t}$ represents the equivalent received signal, $\mathbf{A}_v = [\mathbf{A}_{1,v}, \ldots, \mathbf{A}_{K,v}]$, $\mathbf{G} = \mathrm{blkdiag}\left(\left[\mathbf{g}_{1,t}, \ldots, \mathbf{g}_{K,t}\right]\right)$, and $\mathbf{n}_{v,t} \sim \mathcal{CN}\left(\mathbf{0}, \sigma_n^2\mathbf{I}_M\right)$.

At mmWave frequencies, the NLoS components of the channel gain are typically 5 dB to 10 dB weaker than the LoS components [54], [55]. Leveraging this characteristic, we can distinguish between LoS and NLoS signal contributions. Consequently, the array output can be reformulated to emphasize the LoS components as follows

$$\begin{aligned}\mathbf{y}_{v,t} &= \sum_{k=1}^{K}\mathbf{a}_v\left(\theta_{k,1}\right)g_{k,1,t}s_{k,v,t} + \mathbf{w}_{v,t} \\ &= \mathbf{A}_{v,L}\bar{\mathbf{s}}_{v,L,t} + \mathbf{w}_{v,t}, \end{aligned} \quad (7)$$

where $\mathbf{A}_{v,L} = \left[\mathbf{a}_v\left(\theta_{1,1}\right), \ldots, \mathbf{a}_v\left(\theta_{K,1}\right)\right]$ represents the array steering vector corresponding to the K LoS paths, $\bar{\mathbf{s}}_{v,L,t} = \left[g_{1,1,t}s_{1,v,t}, \ldots, g_{K,1,t}s_{K,v,t}\right]^T$, and $\mathbf{w}_{v,t}$ denotes the interference-plus-noise term. Here, the interference component refers specifically to the NLoS signal contributions, and the complete expression is given by

$$\mathbf{w}_{v,t} = \underbrace{\sum_{k=1}^{K}\sum_{l=2}^{L}\mathbf{a}\left(\theta_{k,l}\right)g_{k,l,t}s_{k,v,t}}_{\text{NLoS interference}} + \underbrace{\mathbf{n}_{v,t}}_{\text{additive noise}}. \quad (8)$$

Due to the significant path loss experienced by NLoS paths and the Gaussian nature of the path gains, the interference-plus-noise term $\mathbf{w}_{v,t}$ can also be approximated as a complex Gaussian distribution.[2] Consequently, the aggregated output of the FA array after G movements, denoted by $\mathbf{y}_t$, is expressed as

$$\mathbf{y}_t = \begin{bmatrix}\mathbf{y}_{0,t}\\ \vdots \\ \mathbf{y}_{G,t}\end{bmatrix} = \begin{bmatrix}\mathbf{A}_{0,L} & & \\ & \ddots & \\ & & \mathbf{A}_{G,L}\end{bmatrix}\begin{bmatrix}\bar{\mathbf{s}}_{0,L,t}\\ \vdots \\ \bar{\mathbf{s}}_{G,L,t}\end{bmatrix} + \mathbf{w}_t, \quad (9)$$

where $\mathbf{w}_t = \left[\mathbf{w}_{0,t}, \ldots, \mathbf{w}_{G,t}\right]^T$. By collecting T snapshots, the FA array output can be expressed in matrix form as $\mathbf{Y}$, given by

$$\mathbf{Y} = \begin{bmatrix}\mathbf{A}_{0,L} & & \\ & \ddots & \\ & & \mathbf{A}_{G,L}\end{bmatrix}\begin{bmatrix}\bar{\mathbf{S}}_{0,L}\\ \vdots \\ \bar{\mathbf{S}}_{G,L}\end{bmatrix} + \mathbf{W}, \quad (10)$$

where $\mathbf{Y} = [\mathbf{y}_1, \ldots, \mathbf{y}_T]$, $\bar{\mathbf{S}}_{v,L} = [\bar{\mathbf{s}}_{v,L,1}, \ldots, \bar{\mathbf{s}}_{v,L,T}]$, and $\mathbf{W} = [\mathbf{w}_1, \ldots, \mathbf{w}_T]$.

In the particular case where the received signals are aligned at the receiver, i.e., $\bar{\mathbf{S}}_L = \bar{\mathbf{S}}_{0,L} = \ldots = \bar{\mathbf{S}}_{G,L}$, (10) can be simplified as follows:

$$\mathbf{Y} = \mathbf{A}_L\bar{\mathbf{S}}_L + \mathbf{W}, \quad (11)$$

where $\mathbf{A}_L = \left[\mathbf{A}_{0,L}^T, \ldots, \mathbf{A}_{G,L}^T\right]^T = [\bar{\mathbf{a}}\left(\theta_{1,1}\right), \ldots, \bar{\mathbf{a}}\left(\theta_{K,1}\right)]$.

Building upon the signal model developed above, the remainder of this paper is organized as follows. In Section III, we will first introduce the design of sparse FA array structures and their corresponding mobility mechanisms. These designs are guided by the array manifold expression $\mathbf{A}_v$ and the concept of consecutive spatial DoFs, which will be formally defined. Subsequently, in Section IV, we will propose two efficient DOA estimation methods tailored to the scenarios described by (10) and (11), respectively.

Remark 1: It should be specifically noted that the two signal models proposed in this paper correspond to distinct physical scenarios: (10) describes the more general scenario with misaligned signals, while (11) represents its specialized and simplified form under aligned signal conditions. The simplification from (10) to (11) is valid when the practical system can complete all spatial sampling within a single channel-coherence time, i.e, when the sampling rate is sufficiently high to treat the channel gains as quasi-static and known pilot sequences are employed. This distinction clarifies the physical implementation requirements and application scenarios corresponding to the different signal models. It is worth

[2]This assumption is commonly adopted in the literature, for instance, in reconfigurable intelligent surface (RIS) assisted localization [56], [57], and is generally considered to align with practical scenarios. Our subsequent simulations will demonstrate that this approximation facilitates improved and more robust DOA estimation.

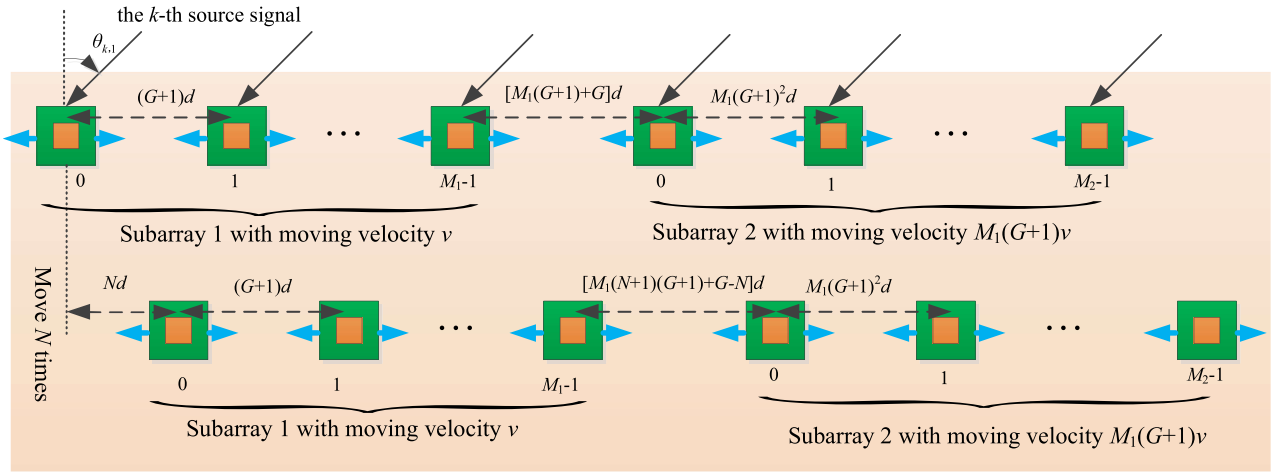

Fig. 2. Sparse FA array structure for aligned received signal scenarios.

emphasizing that one of the central contributions of this work lies in achieving highly efficient spatial sampling through innovative array design and motion strategies, thereby providing crucial technical support for the physical realization of (11).

III. Sparse FA Array Design

This section focuses on the design of sparse reconfigurable array configurations and their associated motion mechanisms. The primary objective is to achieve rapid spatial sampling while circumventing the need for complex motion patterns. Tailored designs are developed for both aligned and misaligned received signal scenarios. These array configurations serve as the foundation for the high-performance, low-complexity DOA estimation algorithms presented in the next section.

Specifically, guided by the core concept of sparse array design that exploits spatial position weighting, we precisely constrain the necessary spatial sampling points to a set of regular motion trajectories, thereby achieving virtual "spacing equivalence" with a physical array. For aligned signals, we design a sparse FA array structure consisting of two subarrays with large element spacing, where different step sizes are applied to the two subarrays to achieve significantly increased consecutive spatial DoFs while avoiding array mutual coupling. For misaligned signals, we propose a generalized FA array which is composed of an FPA array and an FA array with large element spacing, enabling the array output data to be aligned in the second-order statistical domain while still providing increased consecutive spatial DoFs.

A. FA Array Designed for Aligned Received Signals

The FA array designed for aligned received signals consists of two uniform linear subarrays, denoted as subarray 1 and subarray 2, with M_1 and M_2 antenna elements respectively, such that the total number of antenna element is $M = M_1 + M_2$. The design intricacies, illustrated in Fig. 2, are pivotal for maximizing consecutive DoFs. The inter-element spacing within the first subarray is set to $(G+1)d$, while the second subarray features a larger spacing of $M_1(G+1)^2 d$. Here, d is the basic unit of movement, typically half the carrier wavelength. The initial separation distance between the two subarrays is $[M_1(G+1)+G]d$.

A key feature of this configuration is the differential mobility enabled by two independent controllers. Subarray 1 is moved by its controller at a nominal speed v, traversing a distance of d per movement step. Concurrently, subarray 2 is moved by its dedicated controller at a significantly higher speed, $M_1(G+1)v$, covering a distance of $M_1(G+1)d$ in each movement step. For notational convenience, we define $\Delta_1 = G+1$ and $\Delta_2 = M_1(G+1)^2$. Subsequently, the coordinates of the elements in subarray 1 ($\mathcal{P}_N^{(1)}$) and subarray 2 ($\mathcal{P}_N^{(2)}$), as well as the overall array configuration ($\mathcal{P}_N$), after N movements, are given by

$$\mathcal{P}_N^{(1)} = \{N, N+\Delta_1, \ldots, N+(M_1-1)\Delta_1\}\, d, \tag{12}$$

$$\mathcal{P}_N^{(2)} = \{\Delta_{13}^N, \Delta_{13}^N+\Delta_2, \ldots, \Delta_{13}^N+(M_2-1)\Delta_2\} d, \tag{13}$$

$$\mathcal{P}_N = \mathcal{P}_N^{(1)} \cup \mathcal{P}_N^{(2)}, \tag{14}$$

respectively, where $\Delta_{13}^N = (2M_1-1)\Delta_1 + G + M_1 N \Delta_1$.

Definition 1 (Spacing Equivalence and Consecutive Degrees of Freedom): Suppose the elements in an FA array occupy a set of positions $\mathcal{P}$ during the DOA estimation process. We say that the FA array is *spacing equivalent* to an ULA of length $2L+1$ and spacing d if for every $k \in [-L, -L+1, \ldots, L-1, L]$ there exist $p, q \in \mathcal{P}$ such that $p - q = kd$. This implies that the spacing difference k can take $2L+1$ consecutive integer values, defined as the number of consecutive degrees of freedom of the FA array.

The ultimate objective of our design is to construct a dynamic sparse array architecture with deterministic performance guarantees, fundamentally leveraging the reconfigurability of fluid antennas. To simplify motion control, all antennas employ a uniform linear motion pattern. The parametric configuration of each subarray is designed based on the number of movements. In subarray 1, all elements move at the same velocity (i.e., with a uniform step size), the total displacement length is Gd after G displacements, and the initial inter-element spacing is configured as $(G+1)d$. The key rationale behind this design is that it ensures both the uniqueness of sampling positions during movement

and complete coverage of the sampling region. According to the equivalence principle in ***Definition 1***, after G movements, subarray 1 becomes equivalent to a ULA with $L = M_1(G+1)$ elements (considering the positive characteristic).

To maximize the virtual aperture and maintain the continuity of the equivalent virtual array, the parameter configuration and motion strategy of subarray 2 are jointly designed with subarray 1. Specifically, subarray 2 moves at a velocity of $M_1(G+1)v$, aiming to perfectly embed the uniform linear array equivalently generated by subarray 1 into the extended sampling structure constructed by subarray 2. Regarding the inter-element spacing design, the initial spacing of subarray 2 is set as $M_1(G+1)^2 d$. This value aligns with the design concept of subarray 1, ensuring non-overlapping sampling points during motion while significantly enhancing the overall sampling efficiency of the system. Furthermore, for the initial spacing between the two subarrays, we derive the precise analytical expression $[M_1(G+1)+G]d$. This result carries a clear physical interpretation: the first term $M_1(G+1)d$ corresponds to the physical dimension of the equivalent uniform linear array of subarray 1, while the second term Gd represents the total displacement of the rightmost element in subarray 1 throughout the entire motion process. The careful configuration of these spacing parameters provides a crucial guarantee for constructing a seamless virtual array.

Proposition 1: Consider the fluid antenna array designed for aligned received signals in Section III-A, which employs $M = M_1 + M_2$ physical antenna elements. This configuration achieves spacing equivalence to a ULA of length $2(M_1\Delta_1 - 1 + M_1M_2\Delta_1^2) + 1$, corresponding to $L = M_1\Delta_1 - 1 + M_1M_2\Delta_1^2$. To maximize this number of consecutive DoFs for a given total M, the optimal distribution of antennas between the two subarrays is:

- If M is even: $M_1 = M_2 = M/2$;
- If M is odd: $M_1 = (M+1)/2$ and $M_2 = (M-1)/2$ (or vice versa).

Proof: Let $\mathcal{P}^{(1)}$ and $\mathcal{P}^{(2)}$ denote the complete sets of coordinates for all antennas in subarray 1 and subarray 2, respectively, after all possible movements. Specifically, $\mathcal{P}^{(1)}$ is the union of coordinates from all $G+1$ positions of subarray 1, i.e., $\mathcal{P}^{(1)} = \mathcal{P}_0^{(1)} \cup \mathcal{P}_1^{(1)} \cup \cdots \cup \mathcal{P}_G^{(1)}$, where $\mathcal{P}_N^{(1)}$ represents the coordinates of subarray 1 after the N-th movement. Similarly, $\mathcal{P}^{(2)}$ is defined as $\mathcal{P}^{(2)} = \mathcal{P}_0^{(2)} \cup \mathcal{P}_1^{(2)} \cup \cdots \cup \mathcal{P}_G^{(2)}$. After G movements, the coordinate sets can be expressed as:

$$\mathcal{P}^{(1)} = \{\ell d | \ell = 0, 1, \ldots, M_1\Delta_1 - 1\}, \tag{15}$$

$$\mathcal{P}^{(2)} = \{\ell d | \ell = M_1\Delta_1 - 1 + M_1\Delta_1, M_1\Delta_1 - 1 + 2M_1\Delta_1 \ldots, M_1\Delta_1 - 1 + M_1M_2\Delta_1^2\}. \tag{16}$$

In particular, $\mathcal{P}^{(1)}$ will generate $2M_1\Delta_1 - 1$ consecutive DoFs within the range

$$\mathcal{L}_a^{(1)} = [-M_1\Delta_1 + 1, M_1\Delta_1 - 1] \tag{17}$$

$\mathcal{P}^{(2)}$ will generate $2M_2\Delta_1 - 1$ discontinuous DoFs at an interval of $M_1\Delta_1$ within the range

$$\mathcal{L}_a^{(2)} = [-(M_2\Delta_1 - 1)M_1\Delta_1, (M_2\Delta_1 - 1)M_1\Delta_1], \tag{18}$$

and the differences between $\mathcal{P}^{(1)}$ and $\mathcal{P}^{(2)}$ will generate two $M_1M_2\Delta_1^2$ consecutive DoF within the ranges

$$\mathcal{L}_c^{(1)} = [M_1\Delta_1, M_1\Delta_1 - 1 + M_1M_2\Delta_1^2], \tag{19}$$

$$\mathcal{L}_c^{(2)} = [-M_1\Delta_1 + 1 - M_1M_2\Delta_1^2, -M_1\Delta_1], \tag{20}$$

which directly yields $2(M_1\Delta_1 - 1 + M_1M_2\Delta_1^2) + 1$ unique and consecutive spatial DoFs, given by

$$\begin{aligned}\mathcal{L} &= \mathcal{L}_a^{(1)} \cup \mathcal{L}_a^{(2)} \cup \mathcal{L}_c^{(1)} \cup \mathcal{L}_c^{(2)} \\ &= [-M_1\Delta_1 + 1 - M_1M_2\Delta_1^2, M_1\Delta_1 - 1 + M_1M_2\Delta_1^2].\end{aligned} \tag{21}$$

Further define $f = 2(M_1\Delta_1 - 1 + M_1M_2\Delta_1^2) + 1$, then, by replacing M_2 with $M - M_1$ and setting the derivative of f with respect to M_1 equal to zero, we have

$$M_1 = \frac{M}{2} + \frac{1}{2\Delta_1}. \tag{22}$$

Since M_1 is an integer, and $0 < \frac{1}{2\Delta_1} \leq \frac{1}{4}$, provided that $G \geq 1$, the optimal values of M_1 and M_2 are

$$\begin{cases} M_1 = M_2 = \dfrac{M}{2}, & M \text{ is even} \\ M_1 = \dfrac{M+1}{2}, M_2 = \dfrac{M-1}{2}, & M \text{ is odd} \end{cases} \tag{23}$$

and the maximum number of consecutive DoFs are

$$f_{\max} = \begin{cases} M\Delta_1 + \dfrac{M^2\Delta_1^2}{2} - 1, & M \text{ is even} \\ (M+1)\Delta_1 + \dfrac{(M^2-1)\Delta_1^2}{2} - 1, & M \text{ is odd.} \end{cases} \tag{24}$$

This completes the proof of Proposition 1. □

B. FA Array Designed for Misaligned Received Signals

For scenarios involving misaligned received signals, we propose a different FA array architecture termed as a generalized FA array. This configuration comprises two uniform linear subarrays with M_1 and M_2 antenna elements respectively ($M = M_1 + M_2$). While maintaining the same core design philosophy as the aligned signal configuration, the key distinction lies in the composition of the subarrays:

- Subarray 1 is an FPA array with a conventional inter-element spacing of d.
- Subarray 2 is an FA array whose elements are spaced $M_1(G+1)d$ apart.

Unlike conventional approaches that rely solely on algorithmic complexity to achieve high-resolution DOA estimation, the proposed design leverages the intrinsic mobility of FA elements to create additional spatial degrees of freedom through physical movement. By carefully designing the array structure and movement mechanism, the system can achieve a virtual aperture and DoFs expansion that would otherwise require much more complex signal processing algorithms. This hardware-driven approach is a distinctive feature of FAS, enabling high-performance DOA estimation with reduced computational burden and enhanced flexibility, especially in challenging misaligned signal scenarios. Due to the static nature of subarray 1, only subarray 2 is mobile, maneuvered by a single controller at a speed corresponding to $M_1 v$.

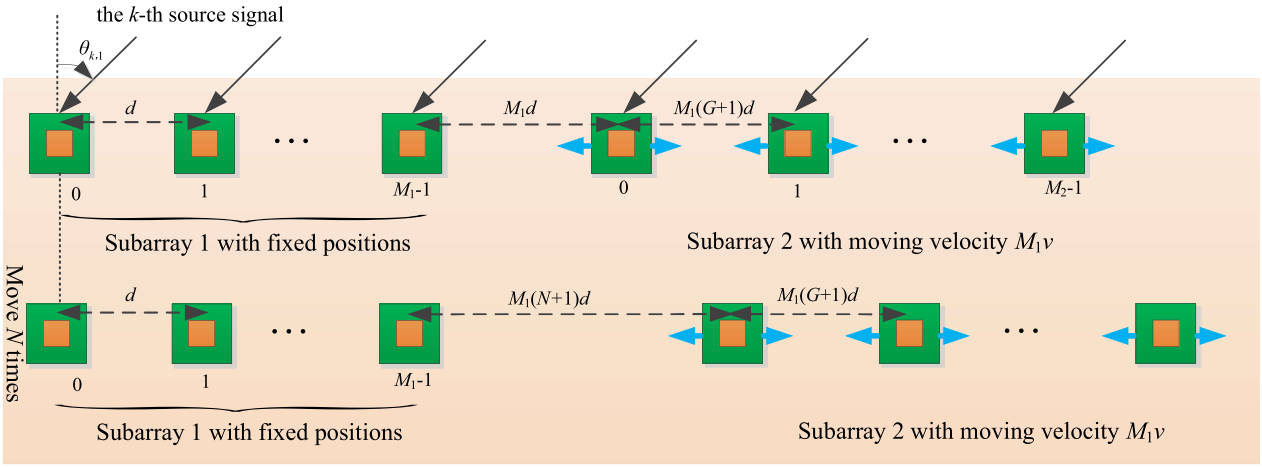

Fig. 3. Sparse FA array structure for misaligned received signal scenarios.

This design, illustrated in Fig. 3, aims to generate substantial consecutive DoFs even without signal alignment across movements. The effectiveness of this design is formalized in ***Proposition 2***.

Proposition 2: For the designed generalized FA array consisting of $M = M_1 + M_2$ antennas and allowing G movements under the scenario of misaligned received signals, the achievable number of consecutive spatial DoFs is $2(M_1 - 1 + M_1M_2\Delta_1) + 1$, corresponding to the range $[-M_1+1-M_1M_2\Delta_1,\ M_1-1+M_1M_2\Delta_1]$. To maximize the number of consecutive DoFs for a given total M, the optimal allocation of antennas between the two subarrays is:

- When M is even: $M_1 = M_2 = \frac{M}{2}$;
- When M is odd: $M_1 = \frac{M+1}{2}$, $M_2 = \frac{M-1}{2}$ (or vice versa).

Proof: After G movements, we have

$$\mathcal{P}^{(1)} = \{\ell d | \ell = 0, 1, \ldots, M_1 - 1\} \tag{25}$$

$$\mathcal{P}^{(2)} = \{\ell M_1 d | \ell = M_1 - 1 + M_1, M_1 - 1 + 2M_1, \ldots, M_1 - 1 + M_2\Delta_1 M_1\}. \tag{26}$$

It can be observed that $\mathcal{P}^{(1)}$ will generate $2M_1 - 1$ consecutive DoFs within the range

$$\mathcal{L}_a^{(1)} = [-M_1 + 1, M_1 - 1] \tag{27}$$

while $\mathcal{P}^{(2)}$ will generate $2M_2\Delta_1 - 1$ discontinuous DoFs at an interval of M_1 within the range

$$\mathcal{L}_a^{(2)} = [-(M_2\Delta_1 - 1)M_1, (M_2\Delta_1 - 1)M_1] \tag{28}$$

and the differences between $\mathcal{P}^{(1)}$ and $\mathcal{P}^{(2)}$ will generate two M_1M_2 consecutive DoFs within the ranges

$$\mathcal{L}_c^{(1)} = [M_1, M_2\Delta_1 M_1 + M_1 - 1] \tag{29}$$

$$\mathcal{L}_c^{(2)} = [-M_2\Delta_1 M_1 - M_1 + 1, -M_1] \tag{30}$$

which directly yields $2(M_1 - 1 + M_1M_2\Delta_1) + 1$ consecutive DoFs, given by

$$\mathcal{L} = \mathcal{L}_a^{(1)} \cup \mathcal{L}_a^{(2)} \cup \mathcal{L}_c^{(1)} \cup \mathcal{L}_c^{(2)} = [-M_1 + 1 - M_1M_2\Delta_1, M_1 - 1 + M_1M_2\Delta_1]. \tag{31}$$

Define $f = 2(M_1 - 1 + M_1M_2\Delta_1) + 1$, and then by using the same partial differentiation way as in proposition 1, the optimal values of M_1 and M_2 can be obtained, which are the same as those in Eq. (23). Finally, the maximum number of consecutive DoFs are

$$f_{\max} = \begin{cases} M - 1 + \dfrac{M^2\Delta_1}{2}, & M \text{ is even} \\ M + \dfrac{(M^2 - 1)\Delta_1}{2}, & M \text{ is odd.} \end{cases} \tag{32}$$

This completes the proof of Proposition 2. □

C. Insights of Two Different Arrays

Several remarks about the designed two FA arrays are given as follows to provide some interesting insights.

Remark 2: From ***Proposition 1*** and ***Proposition 2***, we can observe that the number of consecutive spatial DoFs increases significantly with both G and M. This provides a crucial foundation for achieving high-performance underdetermined DOA estimation. It is worth noting that the minimum requirement for both array designs is two FA units (with $M_1 = M_2 = 1$), which establishes the basic condition for implementing consecutive DoFs extension.

Remark 3: The virtual array configuration resulting from the movement can be viewed as a specialized form of dynamic sparse nested array. However, our design differs fundamentally from conventional FP-based sparse nested arrays by explicitly incorporating the number of movements, G, into both the array structure and movement mechanism. This integration not only achieves higher spatial DoFs but also provides enhanced flexibility. Particularly for aligned signal scenarios, the proposed design offers superior isolation between FA units in the two subarrays, effectively mitigating array mutual coupling effects. This represents a novel approach to improving the performance of wireless communication and signal processing systems.

Remark 4: While the first FA array (designed for aligned signals) achieves a significantly larger number of consecutive spatial DoFs compared to the second array (designed for misaligned signals), the second array offers greater versatility by accommodating both aligned and misaligned signal scenarios. Therefore, when the characteristics of received signals are

unknown, the second FA array design is recommended for its broader applicability.

Remark 5: The number of movements G serves as a primary design parameter and generally needs to be determined before configuring the initial element spacing and velocities. The selection of G is governed by the constrained spatial region, the total number of available fluid antenna elements, and their distribution among subarrays. This parametric dependency introduces an inherent trade-off mechanism in system design, offering substantial flexibility while maintaining practical implementability.

Remark 6: While our work recommends the allocation strategy in (23) to achieve the maximum spatial sampling efficiency, it is important to note that this does not imply that suboptimal allocation strategies are inefficient. On the contrary, even with a suboptimal element allocation, the spatial sampling efficiency of the proposed method can still far surpass that of traditional sequential scanning schemes. This superior performance stems from the core idea of sparse sampling, which inherently distinguishes the "weights" or importance of different spatial sampling locations. Regardless of the specific allocation strategy, our method does not require exhaustive sampling of every possible location within the constrained region. This fundamental property ensures that the proposed framework inherently possesses a much higher sampling efficiency than conventional methods.

IV. DOA Estimation

To achieve robust DOA estimation while maintaining computational efficiency, we propose a closed-form DOA estimator based on LoS path number detection. This approach fully exploits the array output data while minimizing computational complexity. The detailed implementation and performance analysis of this estimator are presented in the following subsections.

A. LoS Path Number Detection Based DOA Estimation

For scenarios with aligned received signals, the array covariance matrix corresponding to the output $\mathbf{Y}$ is expressed as

$$\mathbf{R}_Y = \mathbb{E}\left\{\mathbf{Y}\mathbf{Y}^H\right\} = \mathbf{A}_L\mathbf{R}_s\mathbf{A}_L^H + \mathbf{R}_W, \tag{33}$$

where $\mathbf{A}_L$ represents the array manifold matrix for LoS paths, $\mathbf{R}_s$ denotes the signal covariance matrix, and $\mathbf{R}_W$ accounts for the interference-plus-noise term. The vectorized form of this covariance matrix is given by

$$\mathbf{z} = \mathrm{vec}\left(\mathbf{R}_Y\right) = \tilde{\mathbf{A}}_L\mathbf{b} + \mathrm{vec}\left(\mathbf{R}_W\right), \tag{34}$$

where $\tilde{\mathbf{A}}_L = [\tilde{\mathbf{a}}\left(\theta_{1,1}\right), \tilde{\mathbf{a}}\left(\theta_{2,1}\right), \ldots, \tilde{\mathbf{a}}\left(\theta_{K,1}\right)]$ with its k-th column $\tilde{\mathbf{a}}\left(\theta_{k,1}\right) = \bar{\mathbf{a}}^*\left(\theta_{k,1}\right) \otimes \bar{\mathbf{a}}\left(\theta_{k,1}\right)$. Here, $\mathbf{b} = [p_1, \ldots, p_K]^T$ is a column vector composed of the main diagonal elements of $\mathbf{R}_s$, which is defined as $\mathbf{R}_s = \mathbb{E}\{\bar{\mathbf{S}}_L\bar{\mathbf{S}}_L^H\}$.

Define $\tau = (p-1)MG + q$, $p, q \in [1, MG]$, then the τ-th element of $\tilde{\mathbf{a}}\left(\theta_{k,1}\right)$ is expressed as

$$[\tilde{\mathbf{a}}\left(\theta_{k,1}\right)]_\tau = \exp\left\{j(\tilde{x}_p - \tilde{x}_q)\varpi_{k,1}\right\}, \tag{35}$$

where $\tilde{x}_p$ and $\tilde{x}_q$ represent the virtual coordinates wrt the p-th element in $\bar{\mathbf{a}}^*\left(\theta_{k,1}\right)$ and the q-th element in $\bar{\mathbf{a}}\left(\theta_{k,1}\right)$, respectively.

Based on Proposition 1, we have

$$\{\tilde{x}_p - \tilde{x}_q, p, q \in [1, MG]\} \subseteq \mathcal{L}. \tag{36}$$

This relationship enables us to construct the following observation vector by rearranging the elements in $\mathbf{z}$

$$\begin{aligned}\mathbf{r} &= \mathbf{C}\mathbf{b} + \bar{\mathbf{w}} = \left[\mathbf{c}\left(\theta_{1,1}\right), \ldots, \mathbf{c}\left(\theta_{K,1}\right)\right]\mathbf{b} + \bar{\mathbf{w}} \\ &= \begin{bmatrix} e^{-j\Delta d\varpi_{1,1}} & \cdots & e^{-j\Delta d\varpi_{K,1}} \\ \vdots & \cdots & \vdots \\ 1 & \cdots & 1 \\ \vdots & \cdots & \vdots \\ e^{j\Delta d\varpi_{1,1}} & \cdots & e^{j\Delta d\varpi_{K,1}} \end{bmatrix} \times \begin{bmatrix} p_1 \\ p_2 \\ \vdots \\ p_K \end{bmatrix} + \bar{\mathbf{w}}\end{aligned} \tag{37}$$

where $\Delta = M_1\Delta_1 - 1 + M_1M_2\Delta_1^2$, and $\bar{\mathbf{w}}$ represents the transformed interference-plus-noise term derived from $\mathbf{W}$. For scenarios with misaligned received signals, we obtain a series of sub-covariance matrices, expressed as

$$\mathbf{R}_g = \mathbf{A}_{g,L}\mathbf{R}_{g,L}\mathbf{A}_{g,L}^H + \mathbf{R}_{w,g}, \tag{38}$$

where $\mathbf{R}_{g,L}$ and $\mathbf{R}_{w,g}$ denote the sub-covariance matrices of received signals and noise corresponding to the array output data after the g-th movement.Under the assumption of equal power for transmitted signals and additive noise, we have $\mathbf{R}_{0,L} = \mathbf{R}_{1,L} = \cdots = \mathbf{R}_{G,L}$, and $\mathbf{R}_{w,0} \approx \mathbf{R}_{w,1} \approx \cdots \approx \mathbf{R}_{w,G}$. By incorporating the results from ***Proposition 2***, we can construct an observation vector $\mathbf{r}$ with the same structure as (37), but with a modified Δ (i.e., $\Delta = M_1 - 1 + M_1M_2\Delta_1$) for the misaligned signal scenario.

Next, we divide $\mathbf{r}$ into $\Delta + 1$ overlap sub-vectors, and then construct a $(\Delta+1) \times (\Delta+1)$ matrix, written by

$$\begin{aligned}\mathbf{R}_r &= [\mathbf{J}_{\Delta+1}[\mathbf{r}]_{1:\Delta+1}, \ldots, \mathbf{J}_{\Delta+1}[\mathbf{r}]_{\Delta+1:2\Delta+1}] \\ &= \bar{\mathbf{C}}\mathbf{R}_s\bar{\mathbf{C}}^H + \mathbf{R}_{W'},\end{aligned} \tag{39}$$

where $\mathbf{R}_{W'}$ is constructed by the elements of $\bar{\mathbf{w}}$, and $\bar{\mathbf{C}} = [\bar{\mathbf{c}}\left(\theta_{1,1}\right), \bar{\mathbf{c}}\left(\theta_{2,1}\right), \ldots, \bar{\mathbf{c}}\left(\theta_{K,1}\right)]$, with its k-th column $\bar{\mathbf{c}}\left(\theta_{k,1}\right)$ given by

$$\bar{\mathbf{c}}\left(\theta_{k,1}\right) = \left[0, e^{-jd\varpi_{k,1}}, \ldots, e^{-j\Delta d\varpi_{k,1}}\right]^T. \tag{40}$$

It can seen that $\bar{\mathbf{C}}\mathbf{R}_s\bar{\mathbf{C}}^H$ holds the same structure as that obtained with an $(\Delta+1)$-element PFA based uniform linear array (ULA) under the LoS propagation scenarios, allowing most of existing ULA based solutions can be applied directly. To make a good trade off between computational complexity and DOA estimation accuracy, the eigenvalue detection based polynomial root finding algorithm is exploited here.

Based on the uncorrelated characteristics of channel gains at different time blocks and the expression of $\mathbf{w}_{v,t}$ in Eq. (8), $\mathbf{R}_{W'}$ can be written as

$$\mathbf{R}_{W'} = \tilde{\mathbf{C}}\mathbf{R}_{s'}\tilde{\mathbf{C}}^H + \sigma_n^2\mathbf{I}_{\Delta+1} \tag{41}$$

where $\tilde{\mathbf{C}}$ and $\mathbf{R}_{s'}$ represent the transformed array manifold matrix and received signal power matrix wrt NLoS components, respectively.

According to the properties of eigenvalues for sample array covariance matrices, the following relationship holds [58], [59]:

$$\begin{aligned}\mathrm{spec}(\hat{\mathbf{R}}_r) &= (\alpha_1 \ldots, \alpha_K, \beta_1, \ldots, \beta_{(L-1)K}, \underbrace{0, \ldots, 0}_{1\times(\Delta+1-LK)}) \\ &+ \sigma_n^2(\underbrace{1, \ldots, 1}_{1\times MG}) = \sigma_n^2(\underbrace{\alpha_1/\sigma_n^2+1, \ldots, \alpha_K/\sigma_n^2+1}_{\text{LoS eigenvalues}}) \\ &+ \sigma_n^2(\underbrace{\beta_1/\sigma_n^2+1, \ldots, \beta_{(L-1)K}/\sigma_n^2+1}_{\text{NLoS eigenvalues}}) \\ &+ \sigma_n^2(\underbrace{1, 1, \ldots, 1, 1}_{\text{noise eigenvalues}}) \\ &= (\rho_1, \rho_2, \ldots, \rho_{\Delta+1}) \end{aligned} \tag{42}$$

where $\hat{\mathbf{R}}_r$ represents the sample covariance matrix estimated from T snapshots, α_i and β_j denote the true eigenvalues of $\bar{\mathbf{C}}\mathbf{R}_s\bar{\mathbf{C}}^H$ and $\tilde{\mathbf{C}}\mathbf{R}_{s'}\tilde{\mathbf{C}}^H$, respectively. Due to the significant power difference between LoS and NLoS path gains, a distinct gap exists between $\{\rho_1, \ldots, \rho_K\}$ and $\{\rho_{K+1}, \ldots, \rho_{LK}\}$ regardless of the received SNRs. This characteristic enables us to estimate the number of LoS paths through the following approach

$$\hat{K} = \mathrm{P_{eak}}\left(f_k = \rho_k/\rho_{k+1}\right), k = 1, \ldots, \Delta. \tag{43}$$

Remark 7: Accurate estimation of the number of sources/paths is a crucial prerequisite for DOA estimation. While most existing methods rely on the Akaike's information criterion (AIC) or the minimum description length (MDL) criterion [60], [61], [62], these approaches are primarily designed for detecting the total number of paths. Although our proposed LoS path number estimation algorithm is relatively simple, it proves more effective in achieving accurate and robust DOA estimation performance, as demonstrated in subsequent simulations.

With the estimated number of LoS paths $\hat{K}$, we can perform eigenvalue decomposition (EVD) on $\hat{\mathbf{R}}_r$ to obtain

$$\hat{\mathbf{R}}_r = \mathbf{U}_{s'}\mathbf{\Sigma}_{s'}\mathbf{U}_{s'}^H + \mathbf{U}_{W'}\mathbf{\Sigma}_{W'}\mathbf{U}_{W'}^H \tag{44}$$

where the column of $\mathbf{U}_{s'}$ and $\mathbf{U}_{W'}$ represent the eigenvectors corresponding to the signal subspace and generalized interference-plus-noise subspace bases, respectively. $\mathbf{\Sigma}_{s'}$ and $\mathbf{\Sigma}_{W'}$ are diagonal matrices containing the largest K eigenvalues and remaining small eigenvalues of $\hat{\mathbf{R}}_r$, respectively.

Using the obtained $\mathbf{U}_{W'}$, we can construct the root polynomial as

$$f(z) = \mathbf{p}^T(z^{-1})\mathbf{U}_{W'}\mathbf{U}_{W'}^H\mathbf{p}(z) \tag{45}$$

where $\mathbf{p}(z) = \left[1, z, z^2, \ldots, z^{\Delta}\right]^T$. By identifying the K solutions closest to the unit circle in (45), the DOA angle can be estimated as[3]

$$\hat{\theta}_{k,1} = \arcsin\left(\frac{\lambda}{2\pi d}\angle\hat{z}_k\right), k = 1, 2, \ldots, K. \tag{46}$$

[3]Our work is based on an ideal system model (without explicitly considering factors such as phase noise or movement errors): a simplification that is justified by the current implementation precision of FAS. It should be noted that the proposed method shares the same technical foundation as the classical MUSIC algorithm; therefore, the conclusion in [63] regarding the robustness of classical MUSIC against minor perturbations also applies here. Further exploration of robust DOA estimation under substantial systematic errors will be a promising research direction in the future.

B. Performance Analysis and Appropriate Cramér-Rao Bound

1) Estimation Accuracy: The proposed solutions rely on the polynomial root finding algorithm to achieve DOA estimation. According to the derivation in [64], the mean squared error (MSE) of DOA estimation satisfies

$$\mathbb{E}\left\{\left|\theta_{k,1} - \hat{\theta}_{k,1}\right|^2\right\} = \left(\frac{\lambda}{2\pi d\cos\theta_{k,1}}\right)^2 \frac{\mathbb{E}\left\{\left|z_k - \hat{z}_k\right|^2\right\}}{2\left(\Delta+1\right)} \tag{47}$$

which is proportional to the polynomial root estimation error and inversely proportional to Δ (or precisely M and G). This implies that the DOA estimation performance improves as M and G increase. However, for the polynomial root estimation error, it is impacted by various factors, including the number of snapshots, NLoS components, and additive noise, making its impact on DOA estimation performance more complex. In particular, under the limited snapshot condition, the received signal power when calculating the sub-covariance matrix after each movement is difficult to remain consistent. In the process of constructing $\mathbf{r}$ through elements rearrangement, not only is a subset of elements used, but also a misalignment bias is introduced. Further combining the unavoidable NLoS path components, a fixed bias term will appear in the polynomial root estimation error, which is independent of noise variance. As a result, the MSE "saturates" at this bias point even as the noise variance tends to zero or SNR is sufficiently high, as intuitively verified later by simulations.

2) Computational Complexity: The proposed solutions are closed-form ones, whose main computational complexity arises from the construction of the covariance matrix and eigenvalue decomposition (EVD). For aligned signals, the proposed method constructs one $MG \times MG$ covariance matrix with T snapshots, and performs the EVD on a $(\Delta+1)\times(\Delta+1)$ matrix, therefore it roughly requires $\mathcal{O}\left(M^2G^2T + \frac{3}{4}(\Delta+1)^3\right)$. While for misaligned signals, the proposed method constructs G sub-covariance matrices of size $M \times M$ with T snapshots, and still performs the EVD on a $(\Delta+1)\times(\Delta+1)$ matrix, which totally require $\mathcal{O}\left(GM^2T + \frac{3}{4}(\Delta+1)^3\right)$. In comparison with the spectrum search based methods, such as MUSIC [36] and RARE [37], the proposed solutions avoid the spectral peak search and offer better computational efficiency. In addition, it is necessary to point out that Δ in misaligned signals is much smaller than that for aligned signals, therefore, the DOA estimator for misaligned signals is computationally more efficient.

Remark 8: The performance analysis reveals a fundamental trade-off in FA array design. While increasing M and G theoretically enhances DOA estimation accuracy by expanding the spatial DoFs, practical constraints such as limited snapshots and NLoS effects introduce a performance "ceiling" characterized by the MSE saturation phenomenon. This underscores the importance of our array structures that efficiently exploit the available spatial aperture with minimal FA elements and movements. For time-sensitive applications, the aligned signal design offers superior accuracy, whereas the misaligned signal design provides better computational efficiency without compromising robustness. System designers should weigh these

considerations based on specific application requirements and environmental conditions.

3) Capacity for Underdetermined DOA Estimation: The theoretical foundation for our system's ability to handle underdetermined scenarios stems directly from subspace theory. Analysis of the EVD process reveals a fundamental constraint: at least one eigenvector from the constructed covariance matrix must be reserved for spanning the interference-plus-noise subspace $\mathbf{U}_{W'}$. This constraint establishes an upper bound on the number of detectable LoS paths or targets, specifically $K \leq \Delta$.

The significance of this bound becomes apparent when examining the maximum achievable value of Δ, which can reach $\frac{f_{\max}-1}{2}$. For the aligned signal scenario in particular, we have demonstrated that $f_{\max} \geq 2M+1$ when $G \geq 1$ and $M \geq 2$. This relationship reveals a critical insight: our proposed FA array designs can identify more targets than the number of physical antennas employed, thereby achieving true underdetermined DOA estimation. This capability represents a substantial advantage over conventional fixed-position array systems, which are fundamentally limited by their physical antenna count.

The theoretical capacity for underdetermined estimation derived above is comprehensively validated through our simulation results, which demonstrate reliable estimation of multiple targets using significantly fewer physical antenna elements. This confirms that the proposed FA array architecture efficiently exploits the spatial aperture expansion enabled by controlled antenna mobility.

4) Appropriate Cramér-Rao Bound (CRB): The Cramér-Rao Bound (CRB) provides a fundamental theoretical limit on estimation accuracy, serving as a critical benchmark for evaluating the performance of our proposed methods. A distinguishing feature of our approach is that it focuses solely on DOA estimation for LoS paths, while treating NLoS components as part of the interference-plus-noise term $\mathbf{W}$. This modeling choice is justified by the severe attenuation experienced by NLoS components in mmWave propagation environments.

To facilitate mathematical tractability while maintaining model fidelity, we approximate $\mathbf{W}$ as interference drawn from an isotropic complex Gaussian distribution–an approach that has been successfully employed in related works [56], [57]. For the theoretical performance analysis of underdetermined DOA estimation, we adopt Jansson's CRB framework [65], [66] with uncorrelated prior, which is specifically designed for scenarios where the number of targets exceeds the number of physical antenna elements. Within this framework, the (a,b)-th element of the Fisher Information Matrix (FIM) is expressed as:

$$[\mathbf{F}]_{a,b} = T\mathrm{vec}^H\left(\frac{\partial \mathbf{R}_Y}{\partial \boldsymbol{\varsigma}_a}\right)\boldsymbol{\Psi}\mathrm{vec}\left(\frac{\partial \mathbf{R}_Y}{\partial \boldsymbol{\varsigma}_b}\right), \tag{48}$$

where $\boldsymbol{\Psi} = \mathbf{R}_Y^{-T} \otimes \mathbf{R}_Y^{-T}$ represents the weighted matrix, and $\boldsymbol{\varsigma} = [\theta_{1,1}, \ldots, \theta_{K,1}, \mathbf{p}]$ denotes the parameter vector comprising DOA angles and power parameters.

By defining the gradient matrices $\mathbf{D}_\theta = [\mathrm{vec}(\partial \mathbf{R}_Y/\partial\theta_{1,1}), \ldots, \mathrm{vec}(\partial \mathbf{R}_Y/\partial\theta_{K,1})]$ and $\mathbf{D}_p = [\mathrm{vec}(\partial \mathbf{R}_Y/\partial p_1), \ldots, \mathrm{vec}(\partial \mathbf{R}_Y/\partial p_K)]$, the FIM can be compactly expressed as:

$$\mathbf{F} = T\left[\mathbf{D}_\theta\ \mathbf{D}_p\right]^H \boldsymbol{\Psi}\left[\mathbf{D}_\theta\ \mathbf{D}_p\right]. \tag{49}$$

A crucial theoretical result from [66] indicates that the FIM is invertible when $2K \leq 2\Delta + 1$. This condition not only reinforces the underdetermined estimation capability of our design, but also establishes the mathematical validity of the CRB expression. Under these conditions, the closed-form CRB for DOA estimation is given by:

$$\mathrm{CRB}_\theta = \frac{1}{T}\left\{\mathbf{D}_\theta^H \boldsymbol{\Psi}^{1/2}\mathbf{P}^{\perp}_{\boldsymbol{\Psi}^{1/2}\mathbf{D}_p}\boldsymbol{\Psi}^{1/2}\mathbf{D}_\theta\right\}^{-1}, \tag{50}$$

where $\mathbf{P}^{\perp}_{\mathbf{X}} = \mathbf{I} - \mathbf{X}(\mathbf{X}\mathbf{X}^H)^{-1}\mathbf{X}^H$ denotes the orthogonal projection operator.

V. Simulation Results

In this section, the DOA estimation performance of the proposed two solutions is assessed, and compared with that of the subspace based RARE [37], sparse signal reconstruction based unitary approximate message passing (UMAP) [39], as well as the CRB. Meanwhile, the MDL criterion [61] is also selected to compare the LoS path number estimation performance of the proposed eigenvalue detection based estimator. For DOA estimation, the root mean square error (RMSE) obtained by averaging 500 independent Monte-Carlo trials is adopted to assess the performance of different methods.

We present the simulation setup for both aligned and misaligned signal scenarios. For the aligned scenario, the number of movements is $G = 1$ with the basic moving unit d equal to half the carrier wavelength. The initial coordinates of the three FAs are $\{0, 2, 7\}d$, SNR is set to 10 dB, and the number of snapshots T is 1000. The DOAs of the eleven sources are uniformly spaced from -50° to 50° in 10° increments. For the misaligned scenario, the total number of antennas is four, comprising two FPAs at coordinates $\{0, 1\}d$ and two FAs with initial coordinates $\{3, 7\}d$. Here, SNR is 10 dB, $G = 1$, and $T = 500$. The DOAs of the nine sources are uniformly spaced from -60° to 60° in 15° increments. In both scenarios, the amplitude of channel gain for NLoS components is 10 dB weaker than that for LoS components. All other simulation parameters remain consistent between the two scenarios unless otherwise specified.

In the first simulation, we compare the performance of the proposed LoS path number detection scheme with the conventional MDL-based method under both aligned and misaligned signal scenarios. As shown in Fig. 4, regardless of the scenario, the MDL estimator tends to identify the total number of paths in most cases and lacks robustness. In contrast, the proposed method accurately and robustly estimates the number of LoS paths. These results clearly demonstrate the effectiveness and superiority of the proposed LoS detection approach in discriminating LoS components from mixed path environments.

In the second simulation, we evaluate the underdetermined DOA estimation capability of the proposed method in the aligned signal scenario. Fig. 5(a) shows the results of 50 independent trials for eleven LoS targets. The results demonstrate that the proposed method successfully estimates all eleven targets using only three fluid antennas, validating its strong

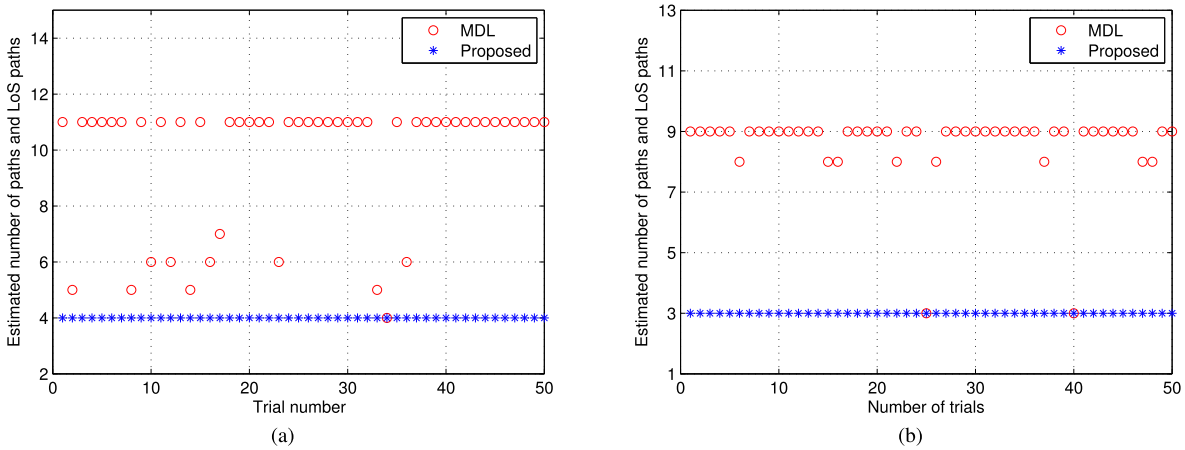

Fig. 4. Comparison of path number estimation strategies: proposed method versus MDL criterion under (a) aligned and (b) misaligned received signals.

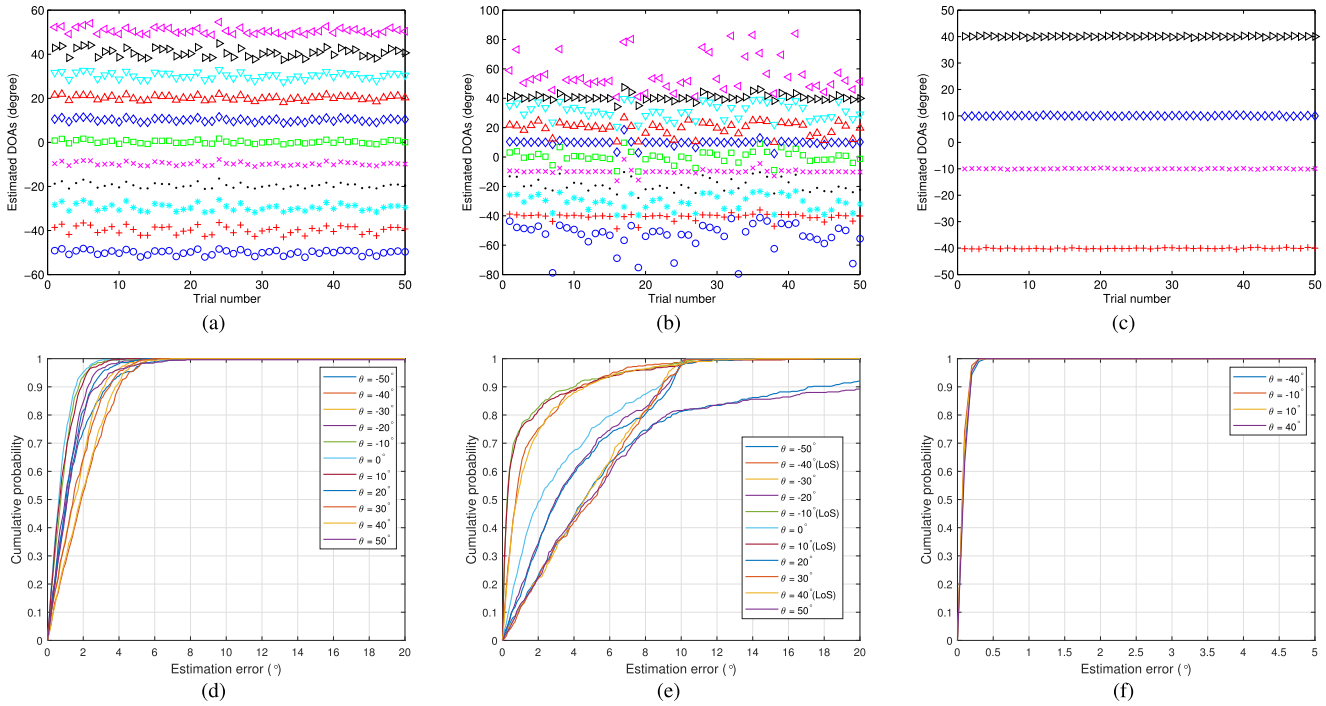

Fig. 5. DOA estimation under aligned signals: (a) Scatter plot for eleven LoS targets; (b) Estimation using total path number; (c) Estimation using LoS path number; (d)-(f) CDF validation of corresponding scenarios.

capability in underdetermined scenarios. In Figs. 5(c) and 5(d), we further compare the DOA estimation performance when using the total number of paths versus the estimated number of LoS paths. The simulation considers four LoS paths with DOAs $\{-40°, -10°, 10°, 40°\}$, while the remaining angles correspond to NLoS paths. The performance comparison reveals that the proposed LoS-based estimator provides significantly improved and more robust DOA estimates, whereas the total path-based approach exhibits considerable bias. To further investigate the statistical characteristics of the estimation performance, we plot the cumulative distribution function (CDF) of the estimation errors based on 500 independent trials. Specifically, Fig. 5(d) presents the CDF corresponding to the scenario in Fig. 5(a), Fig. 5(e) corresponds to Fig. 5(b), and Fig. 5(f) corresponds to Fig. 5(c). All CDF results consistently confirm the validity and statistical significance of the aforementioned conclusions.

In the third simulation experiment, we delve into the underdetermined DOA estimation performance of the proposed method under the more challenging misaligned signal scenario. As shown in Fig. 6(a), our method successfully resolves all targets using merely four antennas, demonstrating its remarkable estimation capability in complex scenarios. We further systematically compare the estimation performance between the strategy based on the total number of paths and that based on the estimated number of LoS paths. In the configured three-path LoS transmission environment (with DOAs of $\{-45°, 0°, 45°\}$), the results in Figs. 6(b)-6(c) clearly

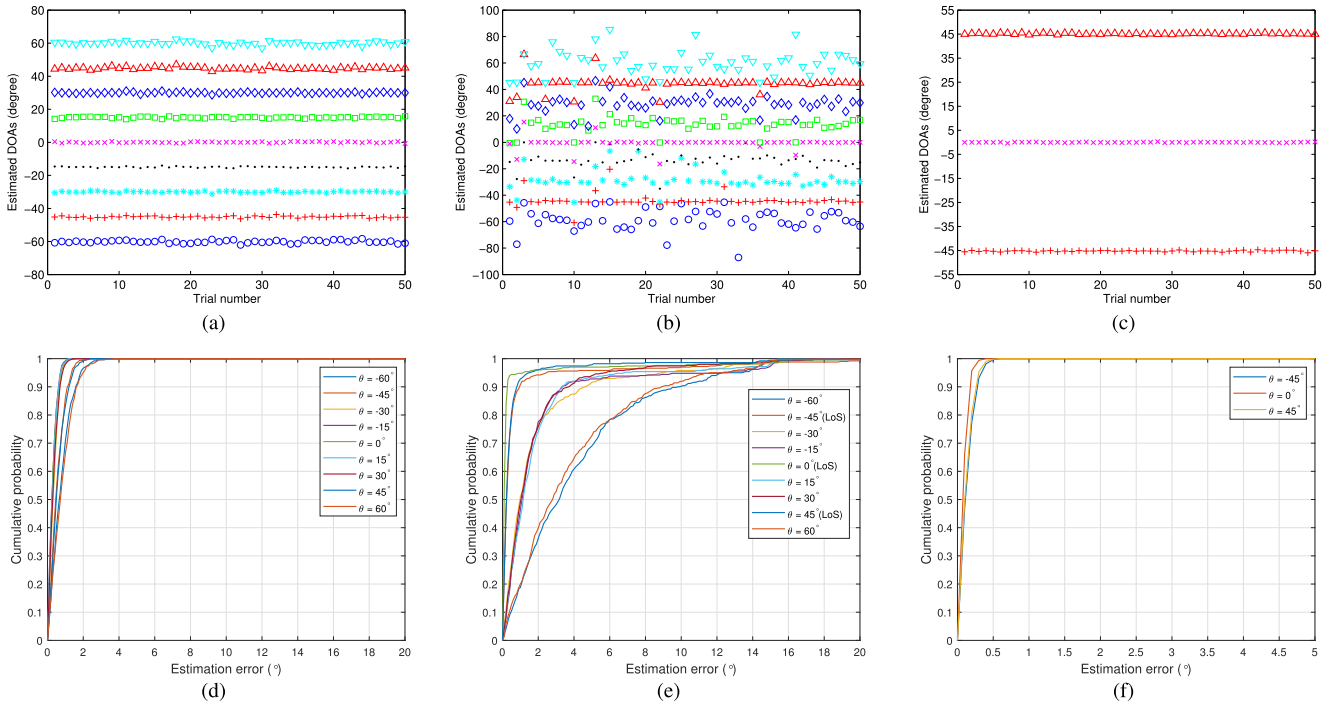

Fig. 6. DOA estimation under misaligned signals: (a) Scatter plot for eleven LoS targets; (b) Estimation using total path number; (c) Estimation using LoS path number; (d)-(f) CDF validation of corresponding scenarios.

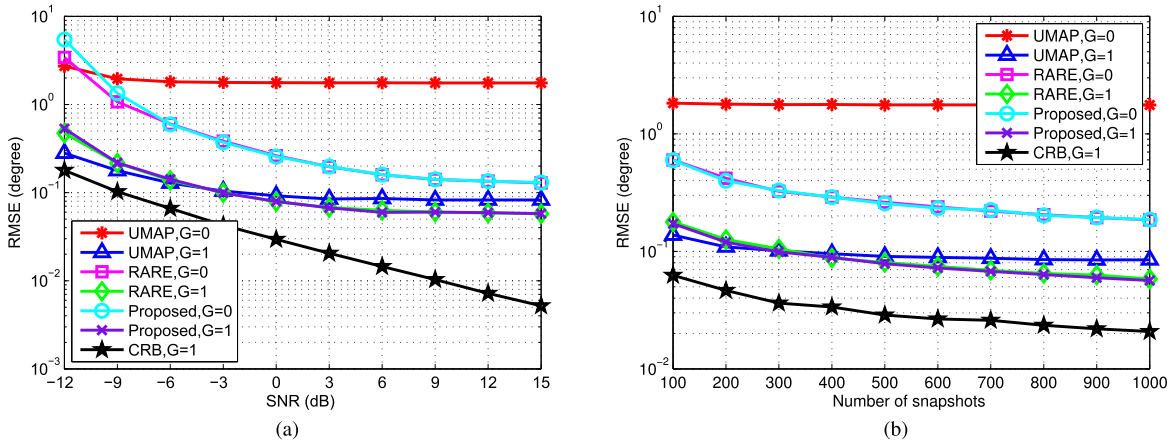

Fig. 7. RMSE of DOA estimation versus SNR and the number of snapshots under the scenario of aligned received signals, $\theta_{1,1} = -20.3°, \theta_{2,1} = 10.7°$, and DOAs wrt NLoS paths are within the range of $[\theta_{k,1} - 5°, \theta_{k,1} + 5°]$: (a) versus SNR; (b) versus the number of snapshots.

reveal that the LoS-based estimator again exhibits significant advantages in both estimation accuracy and result stability, whereas the conventional total-path approach demonstrates noticeable systematic bias. This further validates the practical value of the proposed scheme in real-world millimeter-wave transmission environments. To reinforce the reliability of our conclusions, we similarly construct the cumulative distribution function of the estimation errors based on 500 independent Monte Carlo trials (Figs. 6(d)-6(f)). These CDF curves not only reproduce the advantageous characteristics observed in the aligned scenario but also, from a statistical distribution perspective, confirm the universality and repeatability of the performance gains achieved by the proposed method.

In the fourth simulation, we evaluate the DOA estimation performance under different SNRs and snapshots for the scenario of aligned received signals. Two LoS paths with their DOAs $\theta_{1,1} = -20.3°, \theta_{2,1} = 10.7°$ are considered. For each LoS path, there are two corresponding NLoS paths with corresponding DOAs randomly distributed within the range of $[\theta_{k,1} - 5°, \theta_{k,1} + 5°]$ and amplitudes are attenuated by 10 dB. The initial coordinates of three FAs are $\{0, 2, 7\}d$, and G is set to 0 and 1. In Fig. 7(a), the number of snapshots is fixed at 500, and SNR varies from -12 dB to 15 dB, whereas in Fig. 7(b), SNR is fixed at 0 dB, the number of snapshots varies from 100 to 1000 in steps of 100. As can be seen from the simulation results, the RMSE of DOA estimations decreases

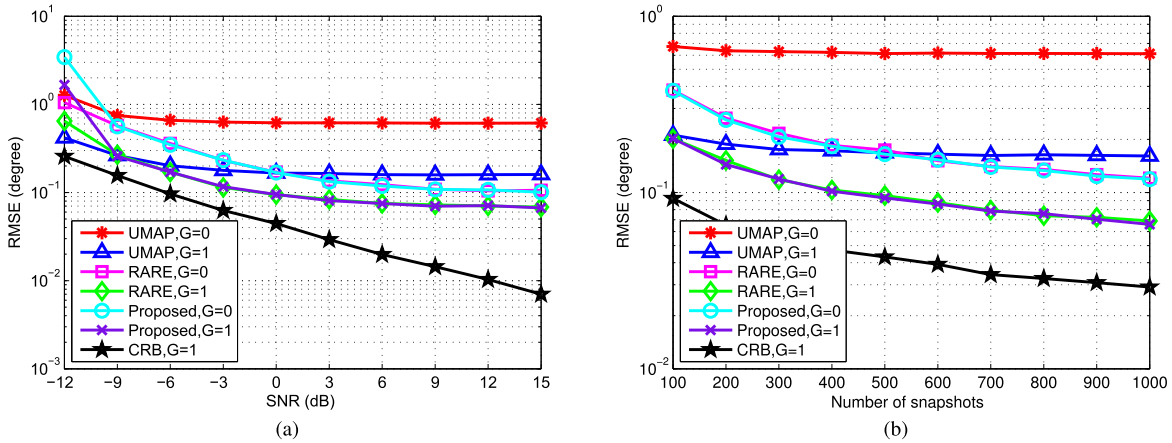

Fig. 8. RMSE of DOA estimation versus SNR and the number of snapshots under the scenario of misaligned received signals, $\theta_{1,1} = -20.3°, \theta_{2,1} = 10.7°$, and DOAs wrt NLoS paths are within the range of $[\theta_{k,1} - 5°, \theta_{k,1} + 5°]$: (a) versus SNR; (b) versus the number of snapshots.

as the increase of the number of movements G, SNR and the number of snapshots, showing the advantage of the designed FA array structure and mobility mechanism efficiently. On the other hand, it can be observed that the proposed polynomial root finding based solution can provide a better estimation performance in comparison with the UMAP when $T > 200$, and almost achieve the same performance with the RARE method. However, as analyzed before, the proposed method belongs to the close-form one, which is computationally more efficient than the RARE method. In addition, it can be further seen that the performance of the proposed solution suffers from "saturation phenomenon", leading a clear gap between the proposed method and CRB in high SNRs, which is consistent with the performance analysis in Section IV.

In the last simulation, we show the RMSEs versus SNR and the number of snapshots under the scenarios of misaligned received signals. The simulation conditions are the same with the third simulation, except that four antennas with two FPAs are located at $\{0, 1\}d$ and two FAs initially are located at $\{3, 7\}d$. It should be noted that the UAMP method is built upon direct processing of the array's time-domain output, while the array structure and motion mechanism designed in this paper aim to achieve generalized signal alignment through the second-order statistical properties of the data. Thus, the UAMP method cannot leverage the proposed virtual aperture expansion mechanism. To ensure a fair performance comparison, the results presented for the UAMP method were obtained under idealized conditions with four fluid antenna elements configured in a classical static nested array geometry (element coordinates at $\{0, 1, 2, 5\}d$ and assuming aligned received signals). As can be seen in Fig. 8, the proposed solution again performs better than the UMAP method, and achieves low complexity and almost the same estimation accuracy with the RARE method, demonstrating the effectiveness of superiority of the proposed solution.

VI. Conclusion

In this paper, we proposed fluid antenna array designs and estimation techniques that offer substantial advantages for DOA estimation in mmWave systems. By intelligently exploiting antenna mobility and sparse array configurations, the framework significantly increases the spatial degrees of freedom, enabling high-resolution DOA estimation even in underdetermined scenarios. Unlike conventional fixed arrays, the proposed approach supports both aligned and misaligned signal conditions while maintaining low complexity and enhanced robustness. These capabilities position fluid antenna systems as a promising hardware-driven solution for next-generation wireless sensing and communication systems, where adaptability, precision, and efficient spatial processing are critical.

References

[1] W. K. New et al., "A tutorial on fluid antenna system for 6G networks: Encompassing communication theory, optimization methods and hardware designs," *IEEE Commun. Surv. Tuts.*, vol. 27, no. 4, pp. 2325–2377, Aug. 2024, doi: 10.1109/COMST.2024.3498855.

[2] T. Wu et al., "Fluid antenna systems enabling 6G: Principles, applications, and research directions," *IEEE Wireless Commun. Mag.*, early access, Dec. 17, 2025, doi: 10.1109/MWC.2025.3629597.

[3] K.-K. Wong, A. Shojaeifard, K.-F. Tong, and Y. Zhang, "Fluid antenna systems," *IEEE Trans. Wireless Commun.*, vol. 20, no. 3, pp. 1950–1962, Mar. 2021.

[4] K.-K. Wong and K.-F. Tong, "Fluid antenna multiple access," *IEEE Trans. Wireless Commun.*, vol. 21, no. 7, pp. 4801–4815, Jul. 2022.

[5] L. Zhu and K.-K. Wong, "Historical review of fluid antenna and movable antenna," 2024, *arXiv:2401.02362*.

[6] X. Lai, T. Wu, J. Yao, C. Pan, M. Elkashlan, and K.-K. Wong, "On performance of fluid antenna system using maximum ratio combining," *IEEE Commun. Lett.*, vol. 28, no. 2, pp. 402–406, Feb. 2024.

[7] X. Lai, J. Yao, K. Zhi, T. Wu, D. Morales-Jimenez, and K.-K. Wong, "FAS-RIS: A block-correlation model analysis," *IEEE Trans. Veh. Technol.*, vol. 74, no. 2, pp. 3412–3417, Feb. 2025.

[8] J. Yao et al., "FAS-RIS communication: Model, analysis, and optimization," *IEEE Trans. Veh. Technol.*, vol. 74, no. 6, pp. 9938–9943, Jun. 2025.

[9] J. Yao et al., "FAS-driven spectrum sensing for cognitive radio networks," *IEEE Internet Things J.*, vol. 12, no. 5, pp. 6046–6049, Mar. 2025.

[10] J. Yao, T. Wu, L. Zhou, M. Jin, C. Huang, and C. Yuen, "FAS versus ARIS: Which is more important for FAS-ARIS communication systems?," *IEEE Trans. Wireless Commun.*, vol. 25, pp. 2075–2091, 2026.

[11] H. Xu et al., "Channel estimation for FAS-assisted multiuser mmWave systems," *IEEE Commun. Lett.*, vol. 28, no. 3, pp. 632–636, Mar. 2024.

[12] F. Rostami Ghadi, K.-K. Wong, F. J. López-Martínez, and K.-F. Tong, "Copula-based performance analysis for fluid antenna systems under arbitrary fading channels," *IEEE Commun. Lett.*, vol. 27, no. 11, pp. 3068–3072, Nov. 2023.

[13] W. K. New, K.-K. Wong, H. Xu, K.-F. Tong, and C.-B. Chae, "An information-theoretic characterization of MIMO-FAS: Optimization, diversity-multiplexing tradeoff and q-outage capacity," *IEEE Trans. Wireless Commun.*, vol. 23, no. 6, pp. 5541–5556, Jun. 2024.

[14] N. Waqar, K.-K. Wong, K.-F. Tong, A. Sharples, and Y. Zhang, "Deep learning enabled slow fluid antenna multiple access," *IEEE Commun. Lett.*, vol. 27, no. 3, pp. 861–865, Mar. 2023.

[15] T. Wu et al., "Scalable FAS: A new paradigm for array signal processing," 2025, *arXiv:2508.10831*.

[16] B. Liu, K.-F. Tong, K.-K. Wong, C.-B. Chae, and H. Wong, "Programmable meta-fluid antenna for spatial multiplexing in fast fluctuating radio channels," *Opt. Exp.*, vol. 33, no. 13, pp. 28898–28915, 2025.

[17] J. Zhang et al., "A novel pixel-based reconfigurable antenna applied in fluid antenna systems with high switching speed," *IEEE Open J. Antennas Propag.*, vol. 6, pp. 212–228, 2025.

[18] S. Qin, Y. D. Zhang, and M. G. Amin, "Generalized coprime array configurations for direction-of-arrival estimation," *IEEE Trans. Signal Process.*, vol. 63, no. 6, pp. 1377–1390, Mar. 2015.

[19] P. Pal and P. P. Vaidyanathan, "Nested arrays: A novel approach to array processing with enhanced degrees of freedom," *IEEE Trans. Signal Process.*, vol. 58, no. 8, pp. 4167–4181, Aug. 2010.

[20] H. Chen, H. Lin, W. Liu, Q. Wang, Q. Shen, and G. Wang, "Augmented multi-subarray dilated nested array with enhanced degrees of freedom and reduced mutual coupling," *IEEE Trans. Signal Process.*, vol. 72, pp. 1387–1399, 2024.

[21] H. Guo, H. Chen, S. Yang, W. Liu, C. Yuen, and H. C. So, "A third-order sparse array design scheme based on second-order sum-difference co-array analysis," *IEEE Trans. Veh. Technol.*, vol. 74, no. 4, pp. 6108–6120, Apr. 2025, doi: 10.1109/TVT.2024.3514195.

[22] H. Xu et al., "Capacity maximization for FAS-assisted multiple access channels," *IEEE Trans. Commun.*, vol. 73, no. 7, pp. 4713–4731, Jul. 2025, doi: 10.1109/TCOMM.2024.3516499.

[23] C. Psomas, G. M. Kraidy, K.-K. Wong, and I. Krikidis, "On the diversity and coded modulation design of fluid antenna systems," *IEEE Trans. Wireless Commun.*, vol. 23, no. 3, pp. 2082–2096, Mar. 2024.

[24] D. Zhang, S. Ye, M. Xiao, K. Wang, M. Di Renzo, and M. Skoglund, "Fluid antenna array enhanced over-the-air computation," *IEEE Wireless Commun. Lett.*, vol. 13, no. 6, pp. 1541–1545, Jun. 2024.

[25] Y. Chen, M. Chen, H. Xu, Z. Yang, K.-K. Wong, and Z. Zhang, "Joint beamforming and antenna design for near-field fluid antenna system," *IEEE Wireless Commun. Lett.*, vol. 14, no. 2, pp. 415–419, Feb. 2025.

[26] L. Zhang, H. Yang, Y. Zhao, and J. Hu, "Joint port selection and beamforming design for fluid antenna assisted integrated data and energy transfer," *IEEE Wireless Commun. Lett.*, vol. 13, no. 7, pp. 1833–1837, Jul. 2024.

[27] Z. Xiao, X. Pi, L. Zhu, X.-G. Xia, and R. Zhang, "Multiuser communications with movable-antenna base station: Joint antenna positioning, receive combining, and power control," *IEEE Trans. Wireless Commun.*, vol. 23, no. 12, pp. 19744–19759, Dec. 2024.

[28] X. Pi, L. Zhu, Z. Xiao, and R. Zhang, "Multiuser communications with movable-antenna base station via antenna position optimization," in *Proc. IEEE Globecom Workshops (GC Wkshps)*, Dec. 2023, pp. 1386–1391.

[29] Z. Xiao et al., "Channel estimation for movable antenna communication systems: A framework based on compressed sensing," *IEEE Trans. Wireless Commun.*, vol. 23, no. 9, pp. 11814–11830, Sep. 2024.

[30] L. Zhu, W. Ma, B. Ning, and R. Zhang, "Movable-antenna enhanced multiuser communication via antenna position optimization," *IEEE Trans. Wireless Commun.*, vol. 23, no. 7, pp. 7214–7229, Jul. 2024.

[31] W. Liu, M. Haardt, M. S. Greco, C. F. Mecklenbräuker, and P. Willett, "Twenty-five years of sensor array and multichannel signal processing: A review of progress to date and potential research directions," *IEEE Signal Process. Mag.*, vol. 40, no. 4, pp. 80–91, Jun. 2023.

[32] Y. Tian, W. Liu, H. Xu, S. Liu, and Z. Dong, "2-D DOA estimation of incoherently distributed sources considering gain-phase perturbations in massive MIMO systems," *IEEE Trans. Wireless Commun.*, vol. 21, no. 2, pp. 1143–1155, Feb. 2022.

[33] H. Xu, M. Jin, and Q. Guo, "Vehicle positioning with unitary approximate message passing-based DOA estimation under exact spatial geometry," *IEEE Internet Things J.*, vol. 11, no. 8, pp. 14938–14948, Apr. 2024.

[34] W. Zuo, J. Xin, W. Liu, N. Zheng, H. Ohmori, and A. Sano, "Localization of near-field sources based on linear prediction and oblique projection operator," *IEEE Trans. Signal Process.*, vol. 67, no. 2, pp. 415–430, Jan. 2019.

[35] S. Liu, W. Wang, L. Fu, and Q. Lu, "Linear prediction-based DOA estimation for directional borehole radar 3-D imaging," *IEEE Trans. Geosci. Remote Sens.*, vol. 57, no. 8, pp. 5493–5501, Aug. 2019.

[36] R. Schmidt, "Multiple emitter location and signal parameter estimation," *IEEE Trans. Antennas Propag.*, vol. AP-34, no. 3, pp. 276–280, Mar. 1986.

[37] F. Wen, J. Wang, J. Shi, and G. Gui, "Auxiliary vehicle positioning based on robust DOA estimation with unknown mutual coupling," *IEEE Internet Things J.*, vol. 7, no. 6, pp. 5521–5532, Jun. 2020.

[38] D. Malioutov, M. Cetin, and A. S. Willsky, "A sparse signal reconstruction perspective for source localization with sensor arrays," *IEEE Trans. Signal Process.*, vol. 53, no. 8, pp. 3010–3022, Aug. 2005.

[39] Z. Yuan, Q. Guo, and M. Luo, "Approximate message passing with unitary transformation for robust bilinear recovery," *IEEE Trans. Signal Process.*, vol. 69, pp. 617–630, 2021.

[40] Y. Tian, S. Liu, W. Liu, H. Chen, and Z. Dong, "Vehicle positioning with deep-learning-based direction-of-arrival estimation of incoherently distributed sources," *IEEE Internet Things J.*, vol. 9, no. 20, pp. 20083–20095, Oct. 2022.

[41] S. Zheng et al., "Deep learning-based DOA estimation," *IEEE Trans. Cogn. Commun. Netw.*, vol. 10, no. 3, pp. 819–835, Jun. 2024.

[42] Z.-M. Liu and Y.-Y. Zhou, "A unified framework and sparse Bayesian perspective for direction-of-arrival estimation in the presence of array imperfections," *IEEE Trans. Signal Process.*, vol. 61, no. 15, pp. 3786–3798, Aug. 2013.

[43] Y. Liu, Z. Zhang, C. Zhou, C. Yan, and Z. Shi, "Robust variational Bayesian inference for direction-of-arrival estimation with sparse array," *IEEE Trans. Veh. Technol.*, vol. 71, no. 8, pp. 8591–8602, Aug. 2022.

[44] H. Huang, J. Yang, H. Huang, Y. Song, and G. Gui, "Deep learning for super-resolution channel estimation and DOA estimation based massive MIMO system," *IEEE Trans. Veh. Technol.*, vol. 67, no. 9, pp. 8549–8560, Sep. 2018.

[45] Y. Tian, Y. Feng, W. Liu, H. Chen, and G. Wang, "Reconfigurable intelligent surface aided DOA estimation by a single receiving antenna," *IEEE Trans. Commun.*, vol. 73, no. 2, pp. 983–994, Feb. 2025.

[46] Y. Chen, L. Yan, C. Han, and M. Tao, "Millidegree-level direction-of-arrival estimation and tracking for terahertz ultra-massive MIMO systems," *IEEE Trans. Wireless Commun.*, vol. 21, no. 2, pp. 869–883, Feb. 2022.

[47] M. Shafi et al., "Microwave vs. millimeter-wave propagation channels: Key differences and impact on 5G cellular systems," *IEEE Commun. Mag.*, vol. 56, no. 12, pp. 14–20, Dec. 2018.

[48] R. W. Heath, N. González-Prelcic, S. Rangan, W. Roh, and A. M. Sayeed, "An overview of signal processing techniques for millimeter wave MIMO systems," *IEEE J. Sel. Topics Signal Process.*, vol. 10, no. 3, pp. 436–453, Apr. 2016.

[49] Q. Qin, L. Gui, P. Cheng, and B. Gong, "Time-varying channel estimation for millimeter wave multiuser MIMO systems," *IEEE Trans. Veh. Technol.*, vol. 67, no. 10, pp. 9435–9448, Oct. 2018.

[50] T. S. Rappaport, R. W. Heath, R. C. Daniels, and J. N. Murdock, *Millimeter Wave Wireless Communications*. Englewood Cliffs, NJ, USA: PrenticeHall, 2014.

[51] Y. Wang, Y. Zhang, Z. Tian, G. Leus, and G. Zhang, "Super-resolution channel estimation for arbitrary arrays in hybrid millimeter-wave massive MIMO systems," *IEEE J. Sel. Topics Signal Process.*, vol. 13, no. 5, pp. 947–960, Sep. 2019.

[52] J. Wang, W. Zhang, Y. Chen, Z. Liu, J. Sun, and C.-X. Wang, "Time-varying channel estimation scheme for uplink MU-MIMO in 6G systems," *IEEE Trans. Veh. Technol.*, vol. 71, no. 11, pp. 11820–11831, Nov. 2022.

[53] L. Zhu, W. Ma, and R. Zhang, "Movable antennas for wireless communication: Opportunities and challenges," *IEEE Commun. Mag.*, vol. 62, no. 6, pp. 114–120, Jun. 2024.

[54] J. N. Murdock, E. Ben-Dor, Y. Qiao, J. I. Tamir, and T. S. Rappaport, "A 38 GHz cellular outage study for an urban outdoor campus environment," in *Proc. IEEE Wireless Commun. Netw. Conf. (WCNC)*, Shanghai, China, Apr. 2012, pp. 3085–3090.

[55] D. Fan et al., "Angle domain channel estimation in hybrid millimeter wave massive MIMO systems," *IEEE Trans. Wireless Commun.*, vol. 17, no. 12, pp. 8165–8179, Dec. 2018.

[56] C. Pan et al., "Intelligent reflecting surface aided MIMO broadcasting for simultaneous wireless information and power transfer," *IEEE J. Sel. Areas Commun.*, vol. 38, no. 8, pp. 1719–1734, Aug. 2020.

[57] B. Teng, X. Yuan, R. Wang, and S. Jin, "Bayesian user localization and tracking for reconfigurable intelligent surface aided MIMO systems," *IEEE J. Sel. Topics Signal Process.*, vol. 16, no. 5, pp. 1040–1054, Aug. 2022.
[58] D. Passemier, Z. Li, and J. Yao, "On estimation of the noise variance in high dimensional probabilistic principal component analysis," *J. Roy. Stat. Soc. Ser. B, Stat. Methodol.*, vol. 79, no. 1, pp. 51–67, Jan. 2017.
[59] Y. Tian, X. Gao, W. Liu, and H. Chen, "Phase compensation-based localization of mixed far-field and near-field sources," *IEEE Wireless Commun. Lett.*, vol. 11, no. 3, pp. 598–601, Mar. 2022.
[60] H. Akaike, "A new book at the statistical model identication," *IEEE Trans. Autom. Control*, vol. AC-19, no. 6, pp. 716–723, Dec. 1974.
[61] J. Rissanen, "Modeling by shortest data description," *Automatica*, vol. 14, no. 5, pp. 465–471, Sep. 1978.
[62] Y. Tian, Z. Zhang, W. Liu, H. Chen, and G. Wang, "Source enumeration utilizing adaptive diagonal loading and linear shrinkage coefficients," *IEEE Trans. Signal Process.*, vol. 72, pp. 2073–2086, 2024.
[63] A. L. Swindlehurst and T. Kailath, "A performance analysis of subspace-based methods in the presence of model errors. I. The MUSIC algorithm," *IEEE Trans. Signal Process.*, vol. 40, no. 7, pp. 1758–1774, Jul. 1992.
[64] H. Krim, P. Forster, and J. G. Proakis, "Operator approach to performance analysis of root-MUSIC and root-min-norm," *IEEE Trans. Signal Process.*, vol. 40, no. 7, pp. 1687–1696, Jul. 1992.
[65] M. Jansson, B. Goransson, and B. Ottersten, "A subspace method for direction of arrival estimation of uncorrelated emitter signals," *IEEE Trans. Signal Process.*, vol. 47, no. 4, pp. 945–956, Apr. 1999.
[66] A. Koochakzadeh and P. Pal, "Cramér–Rao bounds for underdetermined source localization," *IEEE Signal Process. Lett.*, vol. 23, no. 7, pp. 919–923, Jul. 2016.

He Xu received the B.E. and M.E. degrees from the College of Communication Engineering, Jilin University, Changchun, China, in 2010 and 2013, respectively, and the Ph.D. degree from the Faculty of Information Science and Engineering, Ningbo University, in 2024. From 2014 to 2020, she was a Research Assistant with Yanshan University. Since 2024, she has been a Lecturer with the School of Cyber Science and Engineering, Ningbo University of Technology, China. Her main research interests include direction-of-arrival estimation, fluid antenna enabled localization, massive MIMO, and integrated sensing and communication.

Tuo Wu received the B.Eng. degree in telecommunication engineering from South China Normal University, Guangzhou, China, in 2017, the M.S. degree in wireless radio physics from Sun Yat-sen University, Guangzhou, China, in 2021, and the Ph.D. degree from the School of Electronic Engineering and Computer Science, Queen Mary University of London, U.K., in 2024.

From 2024 to 2025, he was a Post-Doctoral Researcher with the School of Electrical and Electronic Engineering, Nanyang Technological University, Singapore. He is currently a Research Fellow with the State Key Laboratory of Terahertz and Millimeter Waves, Department of Electronic Engineering, City University of Hong Kong, Hong Kong. His research interests include fluid antenna systems (FAS), reconfigurable intelligent surface (RIS), and wireless localization and sensing. He is an Editor of IEEE TRANSACTIONS ON COMMUNICATIONS and IEEE WIRELESS COMMUNICATIONS LETTERS. He serves as a Lead Guest Editor for *IEEE Communications Magazine*. He also served as a Guest Editor for IEEE TRANSACTIONS ON COGNITIVE COMMUNICATIONS NETWORKING, *IEEE Network*, and IEEE OPEN JOURNAL OF THE COMMUNICATIONS SOCIETY.

Ye Tian (Senior Member, IEEE) received the B.S. and Ph.D. degrees from the College of Communication Engineering, Jilin University, Changchun, China, in 2009 and 2014, respectively. He was selected as a young top talent by Hebei Provincial Department of Education in 2016 and as a Yongjiang Yucai Leading and Outstanding Talent of Ningbo in 2022. He was a recipient of the Excellent Paper Award in Natural Sciences for the (2021–2022) from Ningbo City. He is currently an Associate Professor with the Faculty of Information Science and Engineering, Ningbo University. He has published over 50 journals and conference papers, held more than ten patents, and authored one book. His research interests include array signal processing, autonomous vehicle positioning, massive MIMO, and large-dimensional random matrix theory.

Ming Jin (Senior Member, IEEE) received the B.E. and Ph.D. degrees in electronic engineering from Xidian University, Xi'an, China, in 2005 and 2010, respectively.

From 2013 to 2014, he was an Associate Researcher with the School of Electrical, Computer and Telecommunications Engineering, University of Wollongong, Wollongong, NSW, Australia. He is currently a Professor with the Faculty of Electrical Engineering and Computer Science, Ningbo University, Ningbo, China. His research interests include cognitive radio, localization, DOA estimation, and UAV detection.

Wei Liu (Senior Member, IEEE) received the B.Sc. degree in space physics and the L.L.B. degree in intellectual property law from Peking University, China, in 1996 and 1997, respectively, the M.Phil. degree from the Department of Electrical and Electronic Engineering, The University of Hong Kong, in 2001, and the Ph.D. degree from the School of Electronics and Computer Science, University of Southampton, U.K., in 2003.

Then, he was a Post-Doctoral Researcher with Southampton University and later with the Imperial College London. From 2005 to 2023, he was a Lecturer/Senior Lecturer with the Department of Electronic and Electrical Engineering, University of Sheffield, U.K., and from 2023 to 2024, he was a Reader with the School of Electronic Engineering and Computer Science, Queen Mary University of London. Since 2024, he has been a Professor with the Department of Electrical and Electronic Engineering, The Hong Kong Polytechnic University. He has published more than 430 journals and conference papers, six book chapters, and two research monographs titled *Wideband Beamforming: Concepts and Techniques* (Wiley, 2010) and *Low-Cost Smart Antennas* (Wiley, 2019), respectively. His research interests cover a wide range of topics in signal processing, with a focus on sensor array signal processing and its various applications, such as robotics and autonomous systems, human–computer interface, radar, sonar, and wireless communications. He is a member of the Applied Signal Processing Systems Technical Committee (2023–2025) of the IEEE Signal Processing Society (SPS); the Digital Signal Processing Technical Committee of the IEEE Circuits and Systems Society [the Chair for (2022–2024)]; and the IEEE SPS Education Board [(2024–2026), the Chair of its Educational Conference Program Committee)]; and a Former Member of the Sensor Array and Multichannel Signal Processing Technical Committee of the IEEE SPS [(the Chair for (2021–2022)], the IEEE SPS Technical Directions Board (2021–2022), and the IEEE SPS Conference Board and its Executive Subcommittee (2022–2023). He also acted as an Associate Editor of IEEE TRANSACTIONS ON SIGNAL PROCESSING, IEEE ACCESS, and *Journal of the Franklin Institute*. He is an Associate Editor of IEEE ANTENNAS AND WIRELESS PROPAGATION LETTERS and the Executive Associate Editor-in-Chief of the *Frontiers of Information Technology and Electronic Engineering*. He is an IEEE Distinguished Lecturer for the Aerospace and Electronic Systems Society (2023–2024).

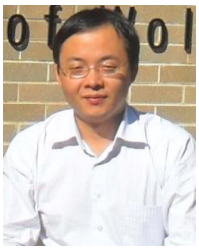

Qinghua Guo (Senior Member, IEEE) received the B.E. degree in electronic engineering and the M.E. degree in signal and information processing from Xidian University, in 2001 and 2004, respectively, and the Ph.D. degree in electronic engineering from the City University of Hong Kong in 2008. He is currently an Associate Professor with the School of Engineering, University of Wollongong, Wollongong, NSW, Australia, and an Adjunct Associate Professor with the School of Engineering, The University of Western Australia, Perth, WA, Australia. His research interests include signal processing, telecommunications, radar, machine learning for signal processing, and optical sensing. He was a recipient of Australian Research Council's inaugural Discovery Early Career Researcher Award in 2012. He serves as an Associate Editor for IEEE TRANSACTIONS ON SIGNAL PROCESSING and IEEE WIRELESS COMMUNICATIONS LETTERS.

Maged Elkashlan (Senior Member, IEEE) received the Ph.D. degree in electrical engineering from The University of British Columbia in 2006. From 2007 to 2011, he was a Scientist with the Commonwealth Scientific and Industrial Research Organization (CSIRO) Australia. During this time, he held visiting faculty appointments with The University of New South Wales, The University of Sydney, and University of Technology Sydney. In 2011, he joined the School of Electronic Engineering and Computer Science, Queen Mary University of London. He also holds a visiting faculty appointment with Beijing University of Posts and Telecommunications. His research interests fall into the broad areas of communication theory and statistical signal processing.

Matthew C. Valenti (Fellow, IEEE) received the M.S. degree from Johns Hopkins University and the Ph.D. degree from Virginia Tech. He is currently a Professor with the Lane Department of Computer Science and Electrical Engineering, West Virginia University. His research focuses on wireless transmission technology, including 5G and beyond wireless systems, multi-antenna and multiuser communications, coded modulation, and advanced signal processing for next-generation networks. He is active in the IEEE Communications Society, where he has served in numerous technical leadership roles, including the Technical Program Chair for IEEE ICC 2024 and IEEE MILCOM 2017 and as the past Chair for the Executive Editorial Committee and Steering Committee of IEEE TRANSACTIONS ON WIRELESS COMMUNICATIONS. He was a recipient of several IEEE Communications Society honors, including the 2025 Harold Sobol Award for Exemplary Service to Meetings & Conferences and the 2019 MILCOM Award for Sustained Technical Achievement. He is a Registered Professional Engineer.

Chan-Byoung Chae (Fellow, IEEE) received the Ph.D. degree in electrical and computer engineering from The University of Texas at Austin (UT), USA, in 2008.

He was a member of Wireless Networking and Communications Group (WNCG), UT. Prior to joining UT, he was a Research Engineer with the Telecommunications R&D Center, Samsung Electronics, Suwon, South Korea, from 2001 to 2005. He is currently an Underwood Distinguished Professor and a Lee Youn Jae Fellow (Endowed Chair Professor) with the School of Integrated Technology, Yonsei University, South Korea. Before joining Yonsei, he was with Bell Laboratories, Alcatel-Lucent, Murray Hill, NJ, USA, from 2009 to 2011, as a member of Technical Staff, and Harvard University, Cambridge, MA, USA, from 2008 to 2009, as a Post-Doctoral Fellow and a Lecturer.

Dr. Chae was a recipient/co-recipient of the Korean Ministry of ICT and Science Award in 2024, the Korean Ministry of Education Award in 2024, the KICS Haedong Scholar Award in 2023, the CES Innovation Award in 2023, the IEEE ICC Best Demo Award in 2022, the IEEE WCNC Best Demo Award in 2020, the Best Young Engineer Award from the National Academy of Engineering of Korea (NAEK) in 2019, the IEEE DySPAN Best Demo Award in 2018, the IEEE/KICS Journal of Communications and Networks Best Paper Award in 2018, the IEEE INFOCOM Best Demo Award in 2015, the IEIE/IEEE Joint Award for Young IT Engineer of the Year in 2014, the KICS Haedong Young Scholar Award in 2013, the IEEE Signal Processing Magazine Best Paper Award in 2013, the IEEE ComSoc AP Outstanding Young Researcher Award in 2012, and the IEEE VTS Dan. E. Noble Fellowship Award in 2008. He has held several editorial positions, including the Editor-in-Chief of IEEE TRANSACTIONS ON MOLECULAR, BIOLOGICAL, AND MULTI-SCALE COMMUNICATIONS, a Senior Editor of the IEEE WIRELESS COMMUNICATIONS LETTERS, and an Editor of IEEE COMMUNICATIONS MAGAZINE, IEEE TRANSACTIONS ON WIRELESS COMMUNICATIONS, and IEEE WIRELESS COMMUNICATIONS LETTERS. He was an IEEE ComSoc Distinguished Lecturer from 2020 to 2023 and is an IEEE VTS Distinguished Lecturer from 2024 to 2025. He is an elected member of the National Academy of Engineering of Korea.

Kin-Fai (Kenneth) Tong (Fellow, IEEE) is currently a Chair Professor in antennas and applied electromagnetics with The Hong Kong Metropolitan University (HKMU), following a 20-year tenure with University College London. His research focuses on novel wideband antennas, circularly polarized patch antennas, fluid antenna systems, surface wave propagation, and microwave/mmWave techniques for 5G/6G and IoT applications. His innovate U.K. project earned an "Outstanding" rating, ranking in the top 5% and featured in the U.K.'s Parliamentary Review. He received the UCL Knowledge Transfer Business of the Year Award in 2015 and the UCL Provost's Spirit of Enterprise Award in 2017. He is a fellow of IET and the Electromagnetics Academy, he serves as a Subject Editor for *IET Electronics Letters* and a Lead Guest Editor for IEEE OPEN JOURNAL OF ANTENNAS AND PROPAGATION. He also chaired IEEE iWEM 2017 and co-chaired IEEE MTT-S workshops.

Kai-Kit Wong (Fellow, IEEE) received the B.Eng., M.Phil., and Ph.D. degrees in electrical and electronic engineering from The Hong Kong University of Science and Technology, Hong Kong, in 1996, 1998, and 2001, respectively. After graduation, he took up academic and research positions with The University of Hong Kong, Lucent Technologies, Bell-Laboratories, Holmdel, the Smart Antennas Research Group of Stanford University, and the University of Hull, U.K. He is currently the Chair in wireless communications with the Department of Electronic and Electrical Engineering, University College London, U.K. His current research centers around 6G and beyond mobile communications. He is a fellow of IET. He served as the Editor-in-Chief for IEEE WIRELESS COMMUNICATIONS LETTERS between 2020 and 2023.